Mon. Not. R. Astron. Soc. **000**, 000–000 (0000) Printed 5 March 2018 (MN LATEX style file v2.2)

Using large galaxy surveys to distinguish $z \simeq 0.5$ quiescent galaxy models

J.D. Cohn[1] and Martin White[2]
[1] *Space Sciences Laboratory and Theoretical Astrophysics Center, University of California, Berkeley, CA 94720,*
[2] *Department of Astronomy and Department of Physics, University of California, Berkeley, CA 94720*

5 March 2018

ABSTRACT

One of the most striking properties of galaxies is the bimodality in their star-formation rates. A major puzzle is why any given galaxy is star-forming or quiescent, and a wide range of physical mechanisms have been proposed as solutions. We consider how observations, such as might be available in upcoming large galaxy surveys, might distinguish different galaxy quenching scenarios. To do this, we combine an N-body simulation and multiple prescriptions from the literature to create several quiescent galaxy mock catalogues. Each prescription uses a different set of galaxy properties (such as history, environment, centrality) to assign individual simulation galaxies as quiescent. We find how and how much the resulting quiescent galaxy distributions differ from each other, both intrinsically and observationally. In addition to tracing observational consequences of different quenching mechanisms, our results indicate which sorts of quenching models might be most readily disentangled by upcoming observations and which combinations of observational quantities might provide the most discriminatory power.

Our observational measures are auto, cross, and marked correlation functions, projected density distributions, and group multiplicity functions, which rely upon galaxy positions, stellar masses and of course quiescence. Although degeneracies between models are present for individual observations, using multiple observations in concert allows us to distinguish between all ten models we consider. In addition to identifying intrinsic and observational consequences of quiescence prescriptions and testing these quiescence models against each other and observations, these methods can also be used to validate colors (or other history and environment dependent properties) in simulated mock catalogues.

1 INTRODUCTION

As time marches forward, collapsed objects in the universe grow hierarchically via merging and accretion. Gas accreting onto halos serves as the fuel for star formation in the galaxies residing in dark matter halos. Not all galaxies are forming stars at a significant rate today however, so a central puzzle in galaxy formation is: why are some galaxies star-forming while others are quiescent? Several possible mechanisms to quench star-forming in galaxies have been identified. For instance, the gas may already be used up in stars, or might be stripped from the galaxies, or prevented from accreting onto them, or heated, and so on (see, e.g., the galaxy formation textbook by Mo, van den Bosch & White 2010). Determining which of these processes are most significant for quenching is a major challenge. Due to the vast range of physical processes and scales which can contribute to the quenching of star-formation (e.g. formation of stars, stellar feedback, and accretion onto and outflows from black-holes) empirical constraints can play a vital role.

Here we consider ways in which large statistical galaxy surveys can be used to distinguish between different models for galaxy quenching, motivated by the tremendous impact of the Sloan Digital Sky Survey (York et al. 2000) on studies of local galaxies, and other large surveys either beginning or being planned. We take such surveys to provide a set of galaxy positions and stellar masses and whether or not the star-formation in the galaxy is quenched. We shall not consider here detailed measurements of individual galaxies on smaller scales, such as galaxy structural properties, properties such as winds, or AGN signatures. While these are indeed valuable, our focus is on properties associated with large-scale structure as is available in large surveys.

We expect that using even relatively little information per galaxy can be highly informative when combined with large statistical samples, because many proposed galaxy quenching mechanisms differ in their dependence upon galaxy formation histories and environments. These differences lead to different overall statistical properties. For example, heating of a galaxy by an AGN may be more likely to occur when the galaxy is in the core of a massive halo, while stripping of gas could be more likely when a galaxy is

moving through a very dense environment (e.g. as a satellite in a massive halo). The two resulting populations have different demographics.

In this work we create mock, quenched galaxy samples in N-body simulations, based upon 10 different models and prescriptions drawn from or motivated by models in the literature. Each model assigns quiescence to individual mock galaxies based upon history and/or environmental criteria, which we expect to be correlated with the underlying physical (and baryonic) processes affecting star-formation. We identify similarities and differences between these models, both intrinsic and observable. Our mock observations of these data help elucidate which future observations might best disentangle such models, and how precise those observations need to be. How the observations interlock and constrain the models is also valuable information for refining mock catalogs – created via any method – which are used in the design and analysis of large surveys.

We shall only consider a single redshift here ($z \simeq 0.5$); while connecting galaxies across time is a powerful technique, it also involves further assumptions. At low redshifts ($z \simeq 0.1$) the wealth of data and in depth analysis of rich data sets such as SDSS (www.sdss.org) has provided many powerful constraints on environments and other properties of quenched galaxies. Some of our models incorporate these insights. By going back to $z \simeq 0.5$, we explore the implications of these mechanisms for a significantly earlier cosmic time, and one for which we expect large statistical samples in the near future[1]. Note that $z \simeq 0.5$ is approximately 5 Gyr ago, which is longer than the main-sequence lifetime of $> 1.4\,M_\odot$ stars. Any galaxy less massive than $2\times10^{10}\,M_\odot$ on the star forming main sequence would at least double its stellar mass in this period[2]. It is also around $z \simeq 0.5$ that we see a rapid rise in the number density of intermediate-mass quiescent galaxies, making this a particularly interesting time to study.

We also focus exclusively on a single galaxy property, quiescence. Comparing measurements for one observed galaxy property, while fixing the others, makes this work similar to the approach of e.g. Hearin & Watson (2013); Masaki, Lin & Yoshida (2013) at $z \simeq 0.1$. This forms a complement to more complex models, such as semi-analytic models, which provide more information on each galaxy across cosmic time but also more dependencies between inputs, assumptions and observations (see e.g. Lu et al. 2010; Neistein & Weinmann 2010; Lu et al. 2013, for recent examples of fitting a suite of parameters in such models to a suite of observations).

The outline of the paper is as follows. In Section 2 we describe the N-body simulation and our observation-based assignments of galaxy stellar mass and total quiescent fraction. In Section 3 we describe our 10 different prescriptions for selecting quiescent galaxies based on histories and environments, and in Section 4 and Section 5 we compare intrinsic and observational properties of the resulting catalogues respectively. Section 7 summarizes and concludes. Throughout we use lg to denote $\log_{10}$, express stellar masses in $M_\odot$ (with no factors of h), and halo masses in units of $h^{-1}M_\odot$. All distances and volumes are comoving and expressed in h^{-1}Mpc or $h^{-3}\,\mathrm{Mpc}^3$.

[1] For example from DES (www.darkenergysurvey.org), HSC (www.naoj.org/Projects/HSC/surveyplan.html), JPAS (j-pas.org), and LSST (www.lsst.org).
[2] Using Eq. (2) of Lilly et al. (2013).

2 SIMULATIONS AND STELLAR MASS ASSIGNMENTS

In order to compare different models and mechanisms for quiescence, we would like to have a sample of mock galaxies with environments, formation histories and stellar masses which are close to what is seen in observations. To this end we associate mock galaxies with dark matter subhalos (defined in more detail below) in an N-body simulation. Such associations are currently the standard tool for analyzing galaxy surveys, as dark matter simulations of the cosmic web are well converged (e.g. Heitmann et al. 2008) and differences between dark matter subhalo definitions and merger trees are becoming similarly well characterized (Onions et al. 2012). The N-body simulation provides subhalo properties such as positions, velocity, (dark matter) mass, environment and history. As dark matter is the dominant contribution to the mass density in the Universe, these quantities are expected to be close approximations[3] to their values when baryons and all interactions are included (a comprehensive simulation of the latter is currently infeasible). We use the terms galaxy and subhalo interchangeably henceforth.

We employ an N-body simulation performed in a periodic box of side $250\,h^{-1}$Mpc. This box has a similar volume to the main galaxy survey of the SDSS, though without boundaries or gaps. At $z \simeq 0.5$ it would subtend around 10° on a side in the plane of the sky. The cosmology is of the ΛCDM family with $(\Omega_m, \Omega_\Lambda, h, n, \sigma_8) = (0.274, 0.726, 0.7, 0.95, 0.8)$. The simulation evolved 2048^3 equal mass particles from initial conditions generated at $z = 150$ with second order Lagrangian perturbation theory, using the code described in White (2002). Phase space data for all of the particles were dumped starting at $z = 10$ and for 45 times equally spaced in $\lg(1+z)$ down to $z = 0$. We use the $z \simeq 0.5$ ($a = 0.676$) output as our observation time. Further details about this simulation can be found in White, Cohn & Smit (2010).

For each output, halos are identified using the Friends of Friends (FoF) algorithm (Davis et al. 1985), with a linking length of 0.168 times the mean inter-particle spacing. Halo masses quoted below are FoF halo masses unless otherwise specified. When halos merge, part of the smaller halo can survive as a self-bound substructure within the larger host halo. In such a situation we call the core of the larger halo the "central subhalo" (or central) of the final system and the core of the smaller halo which "fell in" a "satellite subhalo" (or satellite). We reserve the term "halo" to

[3] There are regimes where the approximation is known to break down, for instance on very small scales where baryons dominate; see Kuhlen, Vogelsberger & Angulo (e.g. 2012) for a recent review. See also Weinberg et al (2008); Simha et al. (2012); van Daalen et al. (2013) for detailed comparisons of subhalo properties with and without baryonic effects.

refer to the parent FoF structure which will host a central subhalo and possibly several satellite subhalos. The subhalos are tracked as overdensities in phase space using the FoF6D algorithm (Diemand, Kuhlen & Madau 2006) as implemented in White, Cohn & Smit (2010). Merger trees and histories are calculated using the methods described in Wetzel, Cohn & White (2009); Wetzel & White (2010).

As in Wetzel & White (2010) we only consider halos (and their descendant subhalos) with masses above $10^{11.3}h^{-1}M_\odot$ to avoid resolution issues (note that subhalos tracked using SUBFIND (Springel, Yoshida & White 2001) require a higher minimum mass cut, as discussed in Guo & White 2012). This cut results in 310,687 galaxies in our $z \simeq 0.5$ box or $\bar{n} = 7 \times 10^{-3}\,\mathrm{Mpc}^{-3}$ (comoving). There are in addition 1, 18 and 110 (roughly cluster sized) halos with mass above $10^{15}h^{-1}M_\odot$, $2 \times 10^{14}h^{-1}M_\odot$ and $10^{14}h^{-1}M_\odot$.

2.1 Stellar mass assignments

Observationally, star formation is correlated with stellar mass, and many of the models we investigate use as an input the stellar mass of the galaxy. We thus need a way to assign stellar masses to our mock galaxies which results in the right demographics and environmental properties. We assign stellar mass to each galaxy using subhalo abundance matching (e.g. Vale & Ostriker 2006; Conroy, Wechsler & Kravtsov 2006) to the $z \simeq 0.5$ stellar mass function of Drory et al. (2009). We use this stellar mass function[4] in part because several of our prescriptions start with the quiescent fractions of central and satellite galaxies proposed by Wetzel et al. (2013a, hereafter WTCB) based upon these data.

We choose to abundance match stellar mass to the maximum mass in a subhalo's history. For a satellite subhalo, this maximum mass is often the mass right before it becomes a satellite, sometimes known as the infall mass. (Using the maximum mass is along the lines recommended by Reddick et al. (2013), who compared several possible abundance matching proxies for stellar masses and luminosities at $z \simeq 0.05$, although the peak velocity was an even better proxy in their case.) We include a 0.16 dex scatter in stellar mass at fixed maximum mass (again motivated by the choices of WTCB) but we clip the scatter at $\pm 2\sigma$ to avoid outliers in the more massive halos which are rare in our simulation box. After assigning $M_\star$, we keep only galaxies with $M_\star \geq 10^{9.5}\,M_\odot$. Of the 310,687 mock galaxies in the box making the halo resolution mass cut, 254,950 then remain (of which 185,532 are central). This galaxy sample is starting point for each of our catalogues below. The stellar mass functions for Drory et al. (2009) and for the simulation box are shown in Fig. 1 where we see good agreement, as expected.

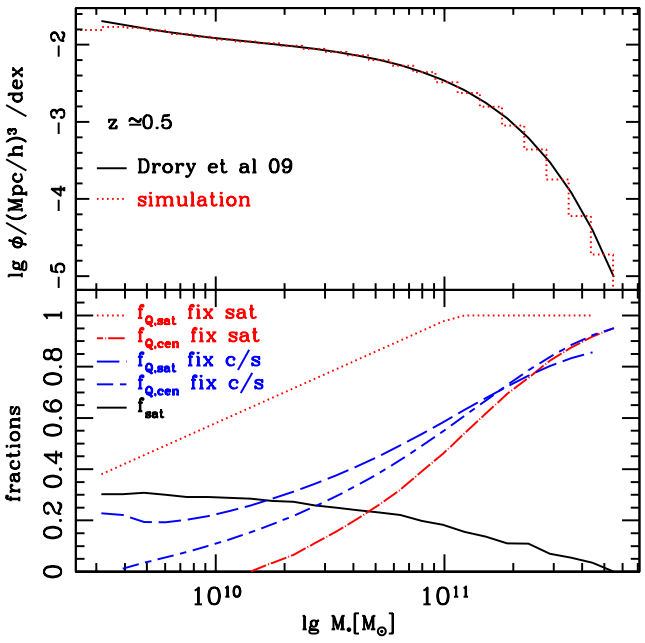

Figure 1. Top: The stellar mass function of Drory et al. (2009, smooth curve) and the histogram (dotted line) of stellar masses in our box. This is used as input to all 10 of our methods. Bottom: Satellite fraction at $z \simeq 0.5$ (solid black line), prescriptions for redshift independent (dotted red line) and dependent (dashed blue line) quiescent satellite fractions, and their corresponding quiescent central fractions. These come from WTCB and are used to construct the "fix sat" and "fix c/s" models described in Section 3.

2.2 Quiescent fraction as a function of stellar mass

Each prescription we consider below assigns a subset of the galaxies in our simulation box to be quiescent. Matching observations of this fraction is clearly a key property, and is built into the specification of several of our models. For example, many of our models are taken from prescriptions of WTCB, which are in turn based upon the Drory et al. (2009) quiescent fraction as a function of stellar mass, $f_{Q,\mathrm{all}}(M_\star)$ (see Fig. 2). Others require a quiescent fraction as function of stellar mass as input, again we choose that of Drory et al. (2009). Specifically, we take $f_{Q,\mathrm{all}}(M_\star)$ as the number of quiescent galaxies divided by the sum of quiescent and active galaxies in the double Schechter function fits of Eq. (1) and Table 3 of Drory et al. (2009).

There is a large diversity in observed quiescent fractions as a function of stellar mass. The origins of some of these differences are understood, in particular, the Drory et al. (2009) quiescent fractions are defined through SED fit-

[4] Several other $z \simeq 0.5$ stellar mass functions exist in the literature including Perez-Gonzales et al. (2008); Ilbert et al. (2010); Pozzetti et al. (2010); Behroozi, Wechsler & Conroy (2013a); Davidzon et al (2013); Knobel et al. (2013); Marulli et al. (2013); Moustakas et al. (2013). These are significantly different and such differences would propagate into the details of our modeling. Some sources of the differences are discussed in Marchesini et al. (2009); Muzzin et al. (2009); Behroozi, Conroy & Wechsler (2010); Ilbert et al. (2010); Moustakas et al. (2013); Tinker et al. (2013). For example, Moustakas et al. (2013) find small effects from changing stellar population synthesis models between FSPS (Conroy, Gunn & White 2009; Conroy, White & Gunn 2010; Conroy & Gunn 2010), Bruzual & Charlot (2003), Maraston (2005), and Pegase (Fioc & Rocca-Volmerange 1997, 1999; Le Borgne et al. 2004), while Behroozi, Conroy & Wechsler (2010) find a shift of 0.1 dex due to the choice of dust model.

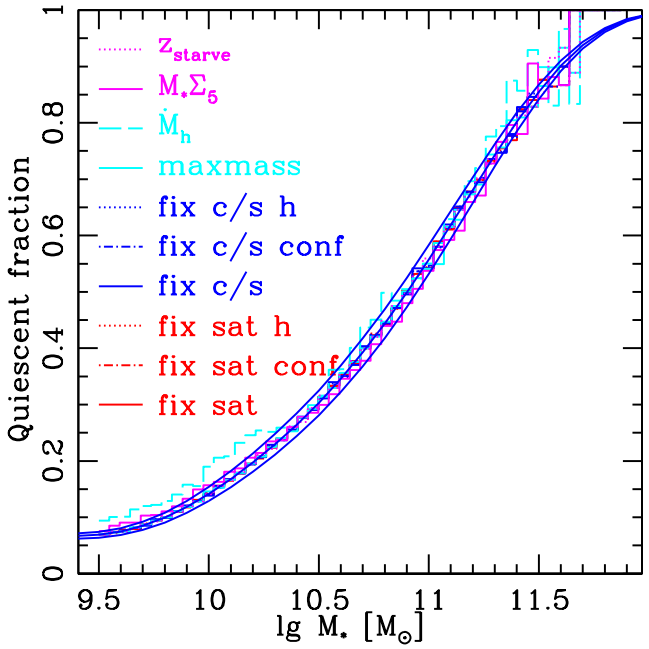

Figure 2. The quiescent fraction in our mock catalogues, all of which are tuned to the Drory et al. (2009) observational fits (smooth blue lines). The central smooth blue line is the ratio of the best-fit quiescent stellar mass function to the quiescent plus active stellar mass functions (from the double Schechter fits in Drory et al. (2009) Eq. (1) and table 3). The two flanking blue curves are the $\pm 1\,\sigma$ variation of the 4 normalizations (ϕ_b and ϕ_f for both quiescent and active galaxies) to give an indication of the range of observational uncertainty. The prescriptions based upon "fix sat", "fix c/s", "maxmass," and $z_{\rm starve}$ all match the Drory et al. (2009) curve by construction, and so are all essentially degenerate. The red lines are for "fix sat" and the blue are for "fix c/s". The solid line is for random quiescent assignment, dot-dashed is our version of galactic conformity ("conf") while dotted is satellite history ("h"). The solid cyan line is the "maxmass" model, while dashed cyan denotes $\dot{M}_h$; magenta solid is $M_\star\,\Sigma_5$ and magenta dotted is $z_{\rm starve}$.

ting, and thus differ from those employing other definitions (e.g. specific star formation rate, color cuts, morphology or some combination). Pozzetti et al. (2010) compare samples of quiescent galaxies selected by several different definitions for a data set at $z \simeq 0.5$. The galaxy samples differ physically and in number density, with color cut based samples tending to include more galaxies because of dust. Two of our models are based upon non-SED based criteria for quiescence. To take this additional (in part definitional) complexity out of our comparisons, we modify our prescriptions, if needed, to improve agreement with the SED based Drory et al. (2009) $f_{Q,\rm all}(M_\star)$. Unfortunately there is not always a unique modification to match to the SED quiescent fraction, or matching it exactly is difficult. We shall discuss these cases in detail below. Our quiescent fraction choice produces approximately 55,000-65,000 quiescent galaxies for each catalogue, depending upon model.

3 PRESCRIPTIONS FOR ASSIGNING QUIESCENT GALAXIES

We now describe the different quiescent galaxy prescriptions we apply and the 10 resulting catalogues.

Our starting point is the $z \simeq 0.5$ box of mock galaxies with stellar masses assigned as described above. (By fixing this underlying galaxy distribution for all 10 catalogues, any differences in quiescent galaxy catalogues are due solely to the differences in assigning quiescence.)

The first and simplest model is motivated by a method by Skibba & Sheth (2009) used at $z \simeq 0.1$ to assign colors to mock galaxies. The method assumes we have a luminosity and central/satellite assignment for each object, and that the color depends only on these properties. Such a method gives good agreement with a number of observations at $z \simeq 0.1$. In our case, we use each galaxy's stellar mass, $M_\star$, and whether it is a satellite or central galaxy to determine the probability that it is quiescent. Individual galaxies are then marked, at random, using these probabilities. With our assumptions, there is only one free function that we must specify to determine the model, and we can take it to be the probability that a satellite galaxy of stellar mass $M_\star$ is quiescent: $f_{Q,\rm sat}(M_\star)$. The central quiescent fraction then is given by the requirement that we match the overall quiescent fraction $f_{Q,\rm all}(M_\star)$ of Drory et al. (2009). In more detail, and because conventions can differ, we define $f_{Q,\rm sat}(M_\star)$ as the fraction of satellites which are quiescent, i.e. the total number of satellite galaxies of a given $M_\star$ which are quiescent is $f_{Q,\rm sat}(M_\star)\,f_{\rm sat}(M_\star)\,N_{\rm gal}(M_\star)$, where $f_{\rm sat}$ is the fraction of $M_\star$ galaxies which are satellites and $N_{\rm gal}(M_\star)$ is the total number of galaxies with stellar mass $M_\star$. The definition of $f_{Q,\rm cen}(M_\star)$ is analogous.

These functions have all been well constrained at $z \simeq 0.1$, but we expect them to change with redshift. Unfortunately, a precise measurement of these functions at higher redshift is difficult as it requires a good group catalog and quiescence classification over a cosmologically representative volume[5]. To overcome this, WTCB suggest extrapolating from $z \simeq 0.1$ to higher z in two ways and using the difference as a measure of uncertainty in the model. As more observations become available we can use the measured $f_{Q,\rm sat}(M_\star)$ rather than these extrapolations. In the meantime, including both models helps us to understand the observational signatures we see later.

3.1 Fixed $f_{Q,\rm sat}$

The first extrapolation to redshift $z = 0.5$, which we refer to as "fix sat", assumes (Wetzel et al. 2013a)

$$\begin{aligned} f_{Q,\rm sat}^{\rm fix\ sat}(M_\star, z=0.5) &\equiv f_{Q,\rm sat}(M_\star, z=0) \\ &= -3.42 + 0.40 \lg M_\star/M_\odot\ . \end{aligned} \quad (1)$$

It is shown for our redshift in Fig. 1 as the dotted (red) line. For the stellar masses of interest to us, the overall quiescent fraction of galaxies is observed to drop rapidly to increasing redshift, while the satellite fraction evolves more modestly

[5] Group catalogues, for small volumes (e.g., Gerke et al. 2012; George et al. 2013), and estimates for associated quiescent fractions (e.g. Knobel et al. 2013; Tinker et al. 2013) are just beginning to be made, based upon a variety of quiescence definitions.

(see e.g. table 1 of Wetzel et al. 2013a, for a recent compilation). If we hold $f_{Q,\rm sat}$ fixed, the decrease in $f_{Q,\rm all}$ must be obtained by decreasing $f_{Q,\rm cen}$. Thus, in order to match the observed evolution of the total quiescent fraction, the fraction of central galaxies which are quiescent in this prescription drops rapidly with increasing redshift.

To implement Eq. (1) and the related models described below, we assign the specified quiescent fractions in 100 bins covering $9.5 \leq \lg M_\star/M_\odot < 12.06$. If either $f_{Q,\rm sat}(M_\star)$ or $f_{Q,\rm cen}(M_\star)$ go outside the region $[0,1]$, we clip its value and choose the other fraction to reach the desired $f_{Q,\rm all}(M_\star)$. For our first prescription, we thus randomly assign galaxies to be quiescent only requiring that Eq. (1) above and the corresponding $f_{Q,\rm cen}(M_\star)$ are satisfied in each stellar mass bin.

We extended this prescription in 2 ways, to get 2 more catalogues. The first extension is a version of "galactic conformity"[6]. The quiescent centrals are taken to be the same as those in the "fix sat" case above. Satellites of quiescent centrals are initially all taken to be quiescent as well. If the resulting number of quiescent satellites is too small to satisfy Eq. (1) in a given $M_\star$ bin, more satellites are randomly assigned to be quiescent. If the number of quiescent satellites is instead too large, quiescent satellites are randomly changed to active to get agreement. Both cases occur, for higher and lower $M_\star$ respectively. (As we shall see later, in a similar model with more quiescent centrals, many more halos have star-forming satellites but quiescent centrals, while there are no cases of quiescent satellites with star-forming centrals. We shall explore the observational consequences of this below.) On average, $\sim 70\%$ of the satellites in high mass halos are quiescent in this variant, compared to about 60% for the (random) "fix sat" model. We call this prescription "fix sat-conf".

We explored a stronger form of galactic conformity as well, which we did not include in our family of catalogues. With our fixed choice of quiescent centrals, inherited from the "fix sat" prescription, we assigned a rank to each halo. Halos with quiescent centrals were ranked first, in order of descending (total) richness. Halos with star-forming centrals followed the centrally quiescent halos but were ranked in ascending order of richness. Each satellite galaxy then inherited the ranking of its parent halo. Within a bin of stellar mass the first ranked $f_{Q,\rm sat}(M_\star)N_{\rm sat}(M_\star)$ of the satellites were marked as quiescent, with the rest being star-forming. This prescription resulted in no star forming galaxies in the richest halos which have quiescent centrals (down to halo masses below $10^{14}h^{-1}M_\odot$). As this is in clear conflict with observations, we work with the less extreme "fix sat-conf" prescription described above.

The second extension based upon Eq. (1), "fix sat-h", introduces a quenching ordering (and thus an implied time scale). Central galaxies from the "fix sat" model are again left unchanged. Each satellite is then ranked by its infall time. To deal with the discreteness in the output times from the simulation we take the infall time to be random, uniformly distributed between the time step when the galaxy was last a central and when it became a satellite.[7] We take some satellites as quiescent upon infall with a probability based on the extrapolations in WTCB for $f_{Q,\rm cen}(M_\star, z)$ in this model as a function of redshift. (They give estimates for 4 stellar mass bins and we extend the redshift scaling of their highest mass bin to apply to the most massive satellites.) We then take the remaining satellites in each stellar mass bin to be quiescent in order of infall time (earliest first) to reach $f_{Q,\rm sat}(M_\star)$ in each stellar mass bin. The quenched satellite which fell in most recently of the latter set determines a quenching time, shown as solid (red) triangles in Fig. 3. (At the highest stellar masses there are very few satellites, leading to the larger scatter in quenching time.)

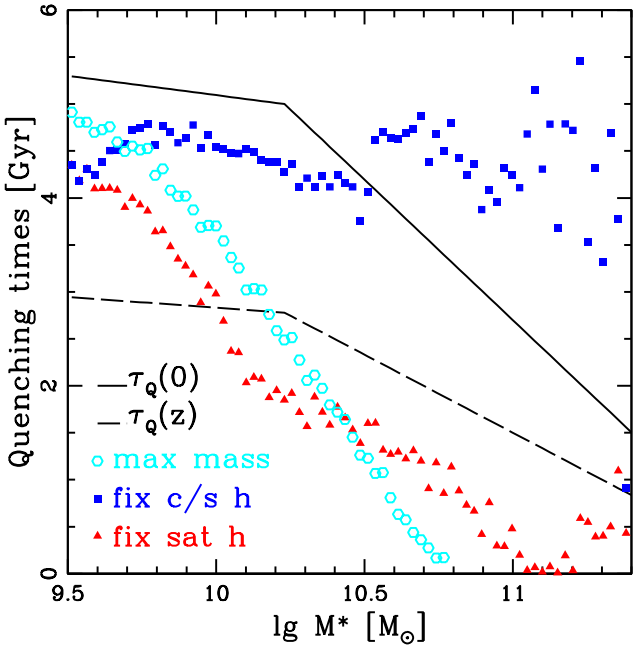

Figure 3. Quenching times found for "fix sat-h" (filled red triangles), "fix c/s-h" (filled blue squares) and "maxmass" (open cyan squares) models as described in the text. The solid black line shows the $z = 0$ quenching times suggested for a model by WTCB which is similar to the "maxmass" model. The (lower) dashed, black line gives a suggested extrapolation to $z = 0.5$ of the $z = 0$ solid line, from Tinker & Wetzel (2010). At the highest stellar masses there are very few satellites, leading to the larger scatter in quenching time.

These first three models differ in how they include environment or history, but the quiescent central galaxies are identical, as is the quiescent satellite fraction as a function of $M_\star$. In particular these models all have a relatively low central quiescent fraction, as a direct consequence of Eq. (1). We now consider the second extrapolation of $f_{Q,\rm cen}(M_*)$ from low redshift of WTCB, to illustrate the impact of this assumption.

[6] Several definitions of conformity are in use, some of which not only affect galaxies sharing the same halo, but also galaxies within a larger region. Ours is most similar to that used by Weinmann et al. (2006) and Ross & Brunner (2009) to describe correlation functions for SDSS at low redshift. See also recent work by Kauffmann et al. (2013); Phillips et al. (2013).

[7] This does add scatter between infall times of galaxies which were part of the same halo when falling into the larger halo, however we expect some scatter as well in the quenching process.

3.2 Fixed $f_{Q,\rm cen}/f_{Q,\rm sat}$

An alternate way to evolve the quiescent satellite fraction, also suggested by WTCB, is to fix not $f_{Q,\rm sat}(M_\star)$ but the ratio of the central and satellite quiescent fractions. To match the observed drop in $f_{Q,\rm all}$ towards higher z, both $f_{Q,\rm sat}$ and $f_{Q,\rm cen}$ decrease. However, since the drop is shared between the two sources this prescription leads to a larger quiescent central fraction than the assumption of Eq. (1). Specifically we take

$$\begin{aligned}\frac{f_{Q,\rm cen}^{\rm fix\ c/s}}{f_{Q,\rm sat}^{\rm fix\ c/s}}(M_\star,z) &\equiv \frac{f_{Q,\rm cen}^{\rm fix\ c/s}}{f_{Q,\rm sat}^{\rm fix\ c/s}}(M_\star,z=0) \\ &= \frac{-6.12+0.64\lg M_\star/M_\odot}{-3.42+0.40\lg M_\star/M_\odot}\ .\end{aligned} \tag{2}$$

Note, for $\lg M_\star/M_\odot < 9.56$ the ratio is negative because the quiescent central fraction at $z=0$ goes negative. For these values of $M_\star$ we take all central galaxies to be active ($f_{Q,\rm cen}(M_\star)\equiv 0$) and set the quiescent satellite fraction to obtain $f_{Q,\rm all}(M_\star)$ of Drory et al. (2009).

We can construct the same three variant models, random, conformity, and satellite infall, using Eq. (2) above as a base instead of Eq. (1) as was done earlier. Some differences are immediately notable. As just described, in comparison to the "fix sat" model, the "fix c/s" model has more (or the same number of) quiescent centrals in all $M_\star$ bins at $z\simeq 0.5$. Due to the increase in number of quiescent centrals relative to the "fix sat" models, the "fix c/s-conf" variation has many more (roughly four times as many) satellites which are active in halos with quiescent centrals, relative to the "fix sat-conf" variation. Furthermore, unlike the "fix sat-conf" case, there are no quiescent satellites in halos with active centrals. We shall see the implications of this below. For the "-h" variation, we again find a the quenching time by assigning galaxies with the earliest infall time as quiescent, but now up to the fraction required by Eq. (2). This quenching time is much longer than that found for the "fix sat" models, hovering above 4 Gyr for almost all stellar masses, as can be seen in Fig. 3. Satellites take longer to quench because many more are quiescent upon infall, and because many fewer are needed as quiescent overall, given Eq. (2).

Further and more detailed comparisons between these prescriptions and our other prescriptions are considered in Sections 4 and 5.

3.3 Other models

Our four other prescriptions for when a galaxy becomes quiescent did not use satellite and central quiescent fractions as a constraint. All are based on models presented in the literature, although we have modified or applied them to obtain the Drory et al. (2009) quiescent fraction $f_{Q,\rm all}(M_\star)$ as a function of stellar mass.

3.3.1 Maximum mass

In the "maxmass" prescription, satellites are quenched in order of the earliest time since their maximum mass, up to the number needed to reach the required $f_{Q,\rm all}(M_\star)$ in each $M_\star$ bin. Similarly to our infall times for satellites, we smooth out the discreteness of the output times in the N-body simulation by assigning the time of maximum mass for each galaxy randomly and uniformly between the relevant bracketing time steps (again this will erase some correlations between galaxies sharing the same halo upon infall). For satellites this maximum mass is also taken to be at or before infall time – we thus exclude mass gains through satellite merging, which can be significant (e.g. Angulo et al. 2009; Simha et al 2009; Wetzel, Cohn & White 2009). This implicitly assumes that mass gains due to merging after infall do not induce further star formation, which seems reasonable. Matching $f_{Q,\rm all}(M_\star)$ in each $M_\star$ bin then determines a quenching time, which is comparable to that of the "fix sat-h" model (open cyan circles and red filled triangles respectively in Fig. 3).

As the time of maximum mass is correlated with the time of first infall into any larger halo (Wetzel et al. 2013b), this model is similar to the WTCB model for quenching. For comparison with their model, we also show their quenching times in Fig. 3, both for $z=0$ (which they use, solid line) and one estimate (Tinker & Wetzel 2010) for the $z\simeq 0.5$ extension (dashed line).

3.3.2 Halo growth

The second of these prescriptions, which we label $\dot{M}_h$, is based on a property of average star formation histories highlighted by Behroozi, Wechsler & Conroy (2013a,b). They calculated the average star formation rate as a function of stellar mass from $0<z<8$, and compared with simulations to find an approximate relation

$$\frac{dM_\star}{dt}\approx\alpha(M_h)f_b\frac{dM_h}{dt} \tag{3}$$

i.e. star formation rate proportional to baryon accretion rate, where the baryon accretion rate is $f_b\,dM_h/dt$ and $f_b = 0.17$ in their cosmology. For $\alpha(M_h)$ independent of redshift, Eq. (3) would imply a redshift-independent $M_\star(M_h)$ relation. While the $M_\star(M_h)$ relation does not evolve strongly, it is not completely redshift independent (e.g. Yang et al. 2012; Wetzel et al. 2013a; Moster, Naab & White 2013; Behroozi, Wechsler & Conroy 2013b; Watson & Conroy 2013), and thus this model can only be an approximation[8]. We make further approximations by using Eq. (3) to estimate the sSFR for individual galaxies and then apply a cut on sSFR to classify a galaxy as quiescent or star-forming, which is similar but not identical to an SED-based classification (as mentioned above, and expanded upon below).

The halo mass change in Eq. (3), dM_h/dt, is the change in $M_{\rm vir}$ halo mass. We approximate the $M_{\rm vir}$ mass gain by the FoF mass gain as the two mass definitions are close at this redshift. In addition, the change in observed stellar mass (the observed star formation rate, of interest to us) has a factor of 1.11 relative to the change in the true stellar mass given above (from Eq. (7) in Behroozi, Wechsler & Conroy (2013a)).

[8] Eq. (3) was also calibrated to simulations with a certain step size which turns out to be different from ours, and thus is approximate for this reason as well. We thank F. van den Bosch for emphasizing this point to us.

Two additional assumptions are needed to identify which galaxies are quiescent. First of all, this approach does not indicate what to do with satellite galaxies. In addition, many central halos have their last significant mass gain earlier than $z \simeq 0.5$. Setting all galaxies in these categories to have zero star formation well exceeds the Drory et al. (2009) quiescent fraction constraint. We instead make an ansatz, again based upon the models in WTCB: we take galaxies to have a star formation rate from their most recent halo mass gain (using dM_h for that step and dt for that step), but if that time is before the present time step, we add a damping factor assuming that the star formation is decaying from an earlier time. (Again, mass gains for satellites after infall, due to merging, are not included.) Following WTCB, we assume star formation actually started at $z = 3$ and that its value at the time of most recent mass gain (given by Eq. 3) has decayed by the time of observation. Taking the star formation history for central galaxies $\propto \Delta t \exp[-\Delta t/\tau_{\rm cen}]$, with $\Delta t = t - t_{\rm form}$ and $t_{\rm form} = t(z = 3)$, WTCB find $\tau_{\rm cen}$ within $1.9 - 3.8\,$Gyr. We take $\tau_{\rm cen} = 3\,$Gyr. The star-formation rate at $z \simeq 0.5$ is then evolved from the value given by Eq. (3) at the time of most recent mass gain using SFR $\propto \Delta t \exp[-\Delta t/\tau_{\rm cen}]$. With only this prescription, however, the model does not have enough quenched galaxies. So in addition to increasing the star formation by using earlier time steps, some quenching is needed to decrease the star formation by the current time. We thus augment the model by setting sSFR $= 10^{-13}\,{\rm yr}^{-1}$ for any central or satellite galaxy which had its more recent mass gain more than a quenching time ago, assuming this quenching time depends upon stellar mass, similar to our earlier models. We have three examples of quenching times from our above constructions: that of the "fix sat-h", "fix c/s-h" and "maxmass" models, in Fig. 3. We chose to use the "fix sat-h" quenching times as they gave the closest agreement to the desired quiescent fraction $f_{Q,{\rm all}}(M_*)$ when combined with the sSFR cut below. (This allows some interesting model comparisons below, as for"fix sat-h" model the times were only defined by and used for the satellites, with centrals were assigned randomly; and here the times are used for all galaxies.) The quenching time is responsible for the quiescence of about 1/5 of the quiescent centrals and about 4/5 of the quiescent satellites (these latter overlap with the "fix sat-h" satellites as a result of using that prescription's time scale).

The last piece needed to get some estimate of quiescence is a comparison of this sSFR estimate to a quiescence classification based on SEDs. The sSFR assignments in WTCB suggest a cut[9] between active and quiescent galaxies at sSFR$= 10^{-11}{\rm yr}^{-1}$. A comparison of SED and sSFR cuts for galaxies at similar redshifts is found in fig. 1 of Pozzetti et al. (2010). Taking those numbers at face value, a sSFR cut of $10^{-11}{\rm yr}^{-1}$ does not include any active galaxies by the SED definition, but also neglects some quiescent ones. We change the maximum specific star formation rate for quiescent galaxies to $3 \times 10^{-11}{\rm yr}^{-1}$, which in Pozzetti et al. (2010) would allow some admixture of active SED galaxies but also includes more quiescent SED galaxies. The resulting galaxy sample gives better agreement numerically with the SED determined quiescent fraction as a function of $M_\star$ in Drory et al. (2009).

Finally, we note that we do not include any scatter in the sSFR, taking it directly from Eq. (3), and we do not self-consistently integrate $dM_\star/dt$ over time, instead applying it instantaneously at $z \simeq 0.5$. A forward integration of Eq. (3) may couple $M_\star$ and $dM_\star/dt$ more closely, while inclusion of scatter would obviously weaken such a correlation.

3.3.3 Stellar mass and density

Our third additional prescription, which we label "$M_\star\,\Sigma_5$", is based on Peng et al. (2010, see also Kovac et al. 2013). These authors found that the red and blue fractions of the zCOSMOS sample could be described by the product of two factors, depending upon projected density Σ_5 and stellar mass,

$$\begin{aligned} f_{\rm red}(M_\star, \Sigma_5) &= \epsilon_{\Sigma_5} + \epsilon_{M_\star} - \epsilon_{\Sigma_5}\epsilon_{M_\star} \\ \epsilon_{\Sigma_5} &= 1 - \exp[(-\Sigma_5/p_1)^{p_2}] \\ \epsilon_{M_\star} &= 1 - \exp[(-M_\star/p_3)^{p_4}]\,. \end{aligned} \qquad (4)$$

with (p_1, p_2, p_3, p_4) functions of redshift. Here Σ_5 is the projected density, defined by fifth nearest neighbor in a redshift cylinder of $\pm 1000\,{\rm km\,s}^{-1}$, including galaxies down to $M_{B,AB} \leq -19.8$ (for $z \simeq 0.5$, Kovac et al. 2010; Peng et al. 2010).

This model is particularly interesting for our purposes because it does not specifically refer to halo mass or to central/satellite designation. However we need to modify it slightly. Although we have $M_\star$ for each galaxy, the projected density assignment as used by Peng et al. (2010) relies upon a sample selected with M_B, and M_B depends upon color, which is related to quiescence, which we are trying to find. In addition, the parameters p_i in Eq. (4) are tuned to separate galaxies into red and blue (i.e. using observations based upon a color cut), rather than quiescent and active. We make two modifications as a result.

Instead of using an M_B-limited sample to define projected density, we use an $M_\star$-limited sample. We choose the minimum $M_\star$ to give the same galaxy number density as the number of galaxies passing the M_B cut of Peng et al. (2010). At $z \simeq 0.5$, the M_B limit is $M_{B,AB} \leq -19.8$. This corresponds to a density of $10^{-2}\,h^3\,{\rm Mpc}^{-3}$ using the COMBO-17, DEEP2 and VVDS B-band luminosity functions quoted in Faber et al. (2007). Matching this number density fixes our threshold $M_\star \simeq 8 \times 10^9 M_\odot$. The projected density Σ_5 is then the inverse square of the distance to the $5^{\rm th}$ nearest neighbor within the cylinder divided by its average value for a sample of random positions within the box.

Using Σ_5 and $M_\star$ in Eq. 4 gives each galaxy in our box a probability of being red, defined by the color cut chosen in Peng et al. (2010). The resulting $f_{Q,{\rm all}}(M_\star)$ well exceeds that of Drory et al. (2009). This is not surprising. As mentioned earlier, color cuts tend to classify more galaxies as quiescent (red) than an SED (our comparison Drory et al.

[9] Note that the bimodality of star formation rates seen in observations (and in WTCB) is not strong in our prescription, as more than half of the quiescent galaxies are such because their mass gains are before $\tau_Q(M_\star)$. The remainder of the quiescent galaxies are just the low end tail of the sSFR distribution. There is a similar issue in Mutch, Croton & Poole (2013).

(2009) sample) or sSFR based cut.[10] Our Σ_5 assignment based upon $M_\star$ rather than M_B might be also a factor, however, this red fraction in our box is a good match to that in Knobel et al. (2013), including central and satellite red fractions as a function of $M\star$. (For this test we also use the Knobel et al. (2013) stellar mass function for consistency.)

Our prescription is thus to keep the form of the Peng et al. (2010) model, but to modify the parameters to match the $f_{Q,\rm all}(M_\star)$ of Drory et al. (2009). As Peng et al. (2010) tuned their parameters using the measured distributions of quiescence as a function of both Σ_5 and $M_\star$, while we only have $f_{Q,\rm all}(M_\star)$, our modifications cannot be unique. (Some degeneracy is expected as there is some correlation of high $M_\star$ with high Σ_5.) We found $(p_1, p_2, p_3, p_4) = (202, 1.71, 1.56 \times 10^{11}, 0.69)$ fit our fiducial $f_{Q,\rm all}(M_\star, z = 0.5)$ quite well, which corresponds to multiplying the Peng et al. (2010) default values (from their table 2, averaged for two redshift bins) by $(3.2, 2.5, 2.5, 1.1)$.

3.3.4 Starvation

Our last prescription is based upon a proposal by Hearin & Watson (2013), see also Zentner, Hearin & van den Bosch (2011), of "age matching". These authors assign r-band luminosities to a simulation similar to ours using subhalo abundance matching, and then order galaxies in luminosity bins according to a redshift $z_{\rm starve}$ (roughly a quenching time). Galaxies with the earliest $z_{\rm starve}$ are taken to be quiescent, up to the total number required (for us set by Drory et al. 2009). Hearin & Watson (2013) define $z_{\rm starve}$ as the maximum (earliest) of three possible redshifts:

-when the host halo equals or exceeds $10^{12}\,h^{-1}M_\odot$.
-when the galaxy becomes a satellite.
-when the host halo growth rate slows down.

Each of these redshifts is taken to be zero if it never occurs. Hearin & Watson (2013) use $M_{\rm vir}$ in the first condition, while we shall instead use $M_{\rm FoF}$. The two definitions are close at the redshifts of interest. The halo growth rate is taken from Wechsler et al. (2002). While Hearin & Watson (2013) use a relation between concentration and halo growth rate, we instead use the definition of Wechsler et al. (2002): $d\log M_{\rm halo}/d\log a \equiv \Delta\log M_{\rm FoF}/\Delta\log a < 2$. We search through the time steps in the simulation to find the earliest time that the halo growth rate dropped below, and subsequently stayed below, the threshold growth rate.

As in our previous models, we bin on $M_\star$ (rather than r-band luminosity). We assign quiescent galaxies based upon the galaxies with the highest $z_{\rm starve}$ in each of 100 stellar mass bins. The last condition (slow down in growth) accounts for slightly more than 60 per cent of the $z_{\rm starve}$, with the remainder of the assignments split approximately equally between the other two conditions.

A fifth additional model which we implemented, but which we do not include below, is that of Lu et al. (2013). These authors assign star formation rate based upon halo mass, infall time for satellites, and stellar mass. Using their preferred model we found quiescent fractions too large to be consistent with Drory et al. (2009). In particular their model had a very short satellite quenching time, making essentially all satellites quenched. While there are combinations of parameters in their prescription which give longer quenching times, without repeating their full likelihood analysis we could not identify combinations which matched the our required quiescent fraction and the other constraints they imposed.[11]

3.4 Summary of the models

The quiescence criteria above result in 10 galaxy catalogues, differing only by which galaxies are marked as quiescent. The next step is to compare measurements on all these catalogues, however it is first useful to summarize how the prescriptions differ. A comparison of the criteria used in determining quiescence (central or satellite in halo, infall time, halo mass change, etc.) is given in Table 1. In words, the criteria for quiescence can be briefly described as:

"fix sat" and "fix c/s" set quiescent satellite and central fractions using Eqs. (1, 2) respectively and $f_{Q,\rm all}(M_*)$, and then assign quiescence randomly

"fix sat-conf" and "fix c/s-conf" as above but put quiescent satellites preferentially in halos with quiescent centrals (the rest are random)

"fix sat-h" and "fix c/s-h" randomly assign some satellites as quiescent at infall using proposed higher redshift behavior, assign rest of quiescent satellites in order of infall time to reach the desired quiescent fraction

"maxmass" assign galaxies which reach their maximum mass the earliest as quiescent, up to the total quiescent fraction desired

$\dot{\mathbf{M}}_{\mathbf{h}}$ take sSFR from most recent halo mass gain; also assign galaxies as quiescent if the most recent halo mass gain is before time scale found in "fix sat-h"

$\mathbf{M}_\star\,\boldsymbol{\Sigma}_{\mathbf{5}}$ quiescent probability from the stellar and (projected) local density using Eq. (4).

$\mathbf{z}_{\rm starve}$ ranks galaxies by earliest of three possible starvation times; assigns quiescence to galaxies in order, up to the number needed.

4 COMPARISONS: INTRINSIC

With these catalogs in hand we wish to see in what ways the different prescriptions lead to different populations of quiescent galaxies. We begin with a discussion of the intrinsic properties, before turning to the observational consequences in Section 5.

Two intrinsic properties are imposed on the catalogues by construction. The first is the stellar mass function, shown in Fig. 1 and implemented identically in all the catalogues. The second, the quiescent fraction of all galaxies as a function of stellar mass, $f_{Q,\rm all}(M_\star)$, was used implicitly or explicitly in the catalogue construction as well (and used to exclude the model of Lu et al. 2013 which did not provide a good match to this function). In Fig. 2, the observations

[10] See also Tinker et al. (2013) for discussion of different quiescent fractions in these models.

[11] We thank Z. Lu for discussions of their work.

Model	cen or sat	sat infall time	$M_h(t)$	nearby galaxies	$\dot{M}_h$
"fix sat" "fix c/s"	x				
"fix sat-conf" "fix c/s-conf"	x			x	
"fix sat-h" "fix c/s-h"	x	x			
"maxmass"	x	(x)	x		
$\dot{M}_h$	x	x			x
$M_\star \Sigma_5$				x	
$z_{\rm starve}$	x	x	x		x

Table 1. Summary of which physical properties were used to assign quiescence for each of the galaxy catalogues. Some catalogues assign quiescence only using whether a galaxy is a central or satellite, in contrast, the $M_\star\,\Sigma_5$ catalog does not refer to host halos at all. Only one model ($z_{\rm starve}$) depends upon host halo mass explicitly. Several models depend upon infall time for satellites, the "maxmass" model only does because mass gain by definition does not happen after infall.

of Drory et al. (2009) are shown along with the measurements from the models. While the models generally reproduce $f_{Q,\rm all}(M_\star)$ quite well, the match is not perfect for all of them. In particular, the $M_\star\,\Sigma_5$ and $\dot{M}_h$ prescriptions have slight excesses at low $M_\star$, and the $\dot{M}_h$ model is also high at high $M_\star$, although in-between it matches the others fairly well.

We now consider measurement other than these two intentionally degenerate properties to highlight differences between the catalogues.

4.1 Central and Satellite Quiescent Fractions

The quiescent fraction of all galaxies as a function of stellar mass, $f_{Q,\rm all}(M_*)$ above, can be decomposed into central and satellite contributions. These are challenging to obtain observationally, which is in part the reason why WTCB propose two different $z \simeq 0.5$ quiescent satellite and central decompositions (the starting points for our "fix sat" and "fix c/s" models). However, understanding the way in which these functions differ between the models will help us to understand the observational trends in the next section, and which observations bear most directly upon this separation.

The breakdowns into quiescent central ($f_{Q,\rm cen}\,f_{\rm cen}$) and quiescent satellite ($f_{Q,\rm sat}\,f_{\rm sat}$) galaxies for our catalogues are shown in Fig. 4. For context we also reproduce the total quiescent galaxy fraction of Drory et al. (2009) from Fig. 2. The solid and dot-dashed lines for the "fix sat" (red) and "fix c/s" (blue) models show the "fix c/s" model almost always has the same number or more quiescent central galaxies than the "fix sat" model, as we have remarked before. This is a direct consequence of the assumed redshift dependence of $f_{Q,\rm sat}$. If the decrease in quenched fraction with increasing redshift is borne entirely by the central galaxies, rather than being shared equally by the central and satellite galaxies, then $f_{Q,\rm cen}$ is very small.

Note that the models separate into two groups, with the $z_{\rm starve}$ prescription lying in-between. The trends in the central, quiescent galaxies are mirrored for the quiescent satellites as the sum is fixed. The models with conformity and the "-h" models have the same fractions as their parent models, because those models simply "shuffle" the quiescent or satellite galaxies into different halos.

Three of the four models which do not specify the satellite and central quiescent fractions directly have strong similarities to the "fix sat" or "fix c/s" models. In part this is because the quenching prescriptions lead to overlap of the quenched populations. The $\dot{M}_h$ model uses the quenching time after satellite infall of the "fix sat-h" model, ∼90 per cent of the $\dot{M}_h$ model quenched satellites coincide with 80 per cent of the "fix sat-h" quenched satellites. The "maxmass" model also has ∼90 per cent of its satellites in common with the "fix sat-h" model (and a similar percentage in common with the $\dot{M}_h$ satellites). These models have much less overlap in their quiescent centrals: quiescent centrals are randomly chosen for "fix sat-h", while those for $\dot{M}_h$ are quiescent because recent mass gain was too small or too long ago, and for "maxmass" because largest mass was too long ago. About 2/3 of the "maxmass" quiescent centrals are also $\dot{M}_h$ centrals, but only about 1/3 of $\dot{M}_h$ and "maxmass" centrals overlap with "fix sat-h" quiescent centrals. As about three times as many central galaxies as satellite galaxies differ between the "maxmass" and $\dot{M}_h$ models relative to the "fix sat" models, central galaxy population differences might be the source of observational differences between the "maxmass" and $\dot{M}_h$ models and the "fix sat" model.

At lower $M_\star$ the satellite fraction is relatively large, and satellites can saturate the required red fraction. Since the halos of central galaxies tend to gain mass more rapidly than those of satellites (whose last mass gain was prior to their infall) the $\dot{M}_h$ and "maxmass" models predict a very small fraction of quiescent, low $M_\star$ centrals.

By contrast, the $M_\star\,\Sigma_5$ model lies close to the initial "fix c/s" fractions. This model has more low-$M_\star$, quiescent centrals than most of the others. In practice, the model makes little distinction between centrals and satellites, as the parameters (p_1, p_2, p_3, p_4) which we found to fit the $f_{Q,\rm all}(M_\star)$ constraint imply $f_{Q,\rm sat}(M_\star) \approx f_{Q,\rm cen}(M_\star)$. These fractions are also fairly close for the "fix c/s" models in Fig. 1. If the satellite and central quiescent fractions are close, more central galaxies will be quiescent because they outnumber satellites at any given $M_\star$. (This satellite/central blindness is not necessarily part of the $M_\star\,\Sigma_5$ form for assigning quiescence. At fixed stellar mass, there is a Σ_5 difference on average between satellites and centrals, and parameters such as those in Peng et al. (2010) can lead to a large difference between $f_{Q,\rm sat}(M_\star)$ and $f_{Q,\rm cen}(M_\star)$.) But by sampling a wide range of parameters, it seems that getting $f_{Q,\rm all}(M_\star)$ low enough at low $M_\star$ requires raising p_1 at low $M_\star$, thus taking $f_{Q,\rm sat}(M_\star)$ towards $f_{Q,\rm cen}(M_\star)$ as we found.)

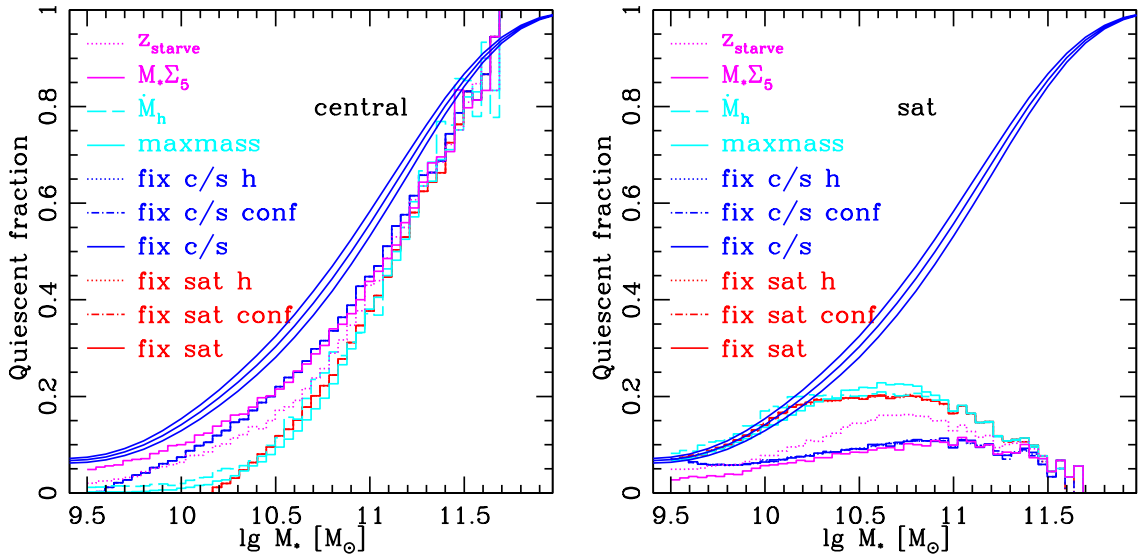

Figure 4. Contributions to the total quiescent fraction from central (left) and satellite (right) quiescent galaxies, as a function of stellar mass. Line types for each of the catalogues are as in Fig. 2, as are the smooth blue lines representing an observational range for the total quiescent fraction. The prescriptions roughly separate into two groups for both central and satellite galaxies, with the $z_{\rm starve}$ prescription lying in-between. The "fix c/s" prescription lies in the group with more quiescent central galaxies as a function of $M_\star$, while the "fix sat" prescription is in the group with fewer quiescent central galaxies. (The trend is reversed for the satellite quiescent galaxies, as the sum is fixed).

We now turn from quiescent satellite and central stellar mass functions to the question of which halos these satellites and central galaxies occupy.

4.2 Quiescent Galaxy Halo Occupation

The manner in which the low- and high-mass quiescent central and satellite galaxies are distributed among halos differs significantly between the models. In this section we ask: "in which types of halos are quiescent galaxies found?"

Fig. 5 shows the average number of quiescent galaxies per halo (the "halo occupation number" or HON; Peacock & Smith 2000; Seljak 2000; Cooray & Sheth 2002), as a function of halo mass. At left we plot all quiescent galaxies, at right only central quiescent galaxies. The average number of all galaxies per halo is also shown for reference as the black line (and is the same for all models). The quiescent fraction as a function of halo mass is just the ratio of each model line to this black line, it is largest at high mass for the "fix sat-conf", "maxmass" and $\dot{M}_h$ models. (The active galaxy HON – the difference of the black solid line and any of the other curves – follows a rising power law for all of the models as well[12]).

As was the case for the quiescent fractions, the quiescent galaxy HON's split roughly into two groupings, which cross around $M_h \simeq 2\times10^{12}\,h^{-1}M_\odot$.

The "fix c/s" model has more quiescent, central galaxies at low $M_\star$ than the "fix sat" model. This in turn implies more quiescent galaxies in low mass halos and a shallower HON. Within the "fix sat" and "fix c/s" classes, the "-conf" models have more quiescent satellites in more massive halos, as these are the halos most likely to host quiescent centrals. Similarly, the "-h" models have more quiescent galaxies in massive halos than their random counterparts because such halos typically host more satellites (of a given stellar mass) that fell in long ago – arising from a combination of reduced dynamical friction and earlier halo formation time. A similar effect operates for the "maxmass" prescription, because satellites which have reached their highest mass long ago tend to have fallen in long ago, and thus are again more prevalent in high mass halos.

The $M_\star\,\Sigma_5$ model HON again seems very similar to the random "fix c/s" model. In both, the satellite and central quiescent fractions are much closer to each other than the other models. This large central quiescent fraction at low $M_\star$ can be seen in Fig. 4 for both models. Since low $M_\star$ centrals live in low mass halos, this in turn explains the low M_h behavior of the HON. Again, this behavior seems to be built into the $M_\star\,\Sigma_5$ model by requiring the form of Eq. (4) to have low enough quiescent fraction at low $M_\star$ (to match our Drory et al. (2009) constraint).[13]

It is notable that the quiescent galaxy richness of clusters can vary by over a factor of two, i.e. the quiescent galaxy HON is very model dependent. This implies that the HON, or the cluster luminosity function for clusters of a wide range of masses, can provide a strong discriminant between models (this has been considered in e.g. Tinker et al. 2012). The differences in the number of quiescent galaxies as a function

[12] We thank P. Behroozi for discussing this measurement with us.

[13] Even though quiescence tends to go with high density and satellites tend to have higher densities, there are many more low density centrals at low $M_\star$, which somewhat cancel out the preference for quiescent satellites.

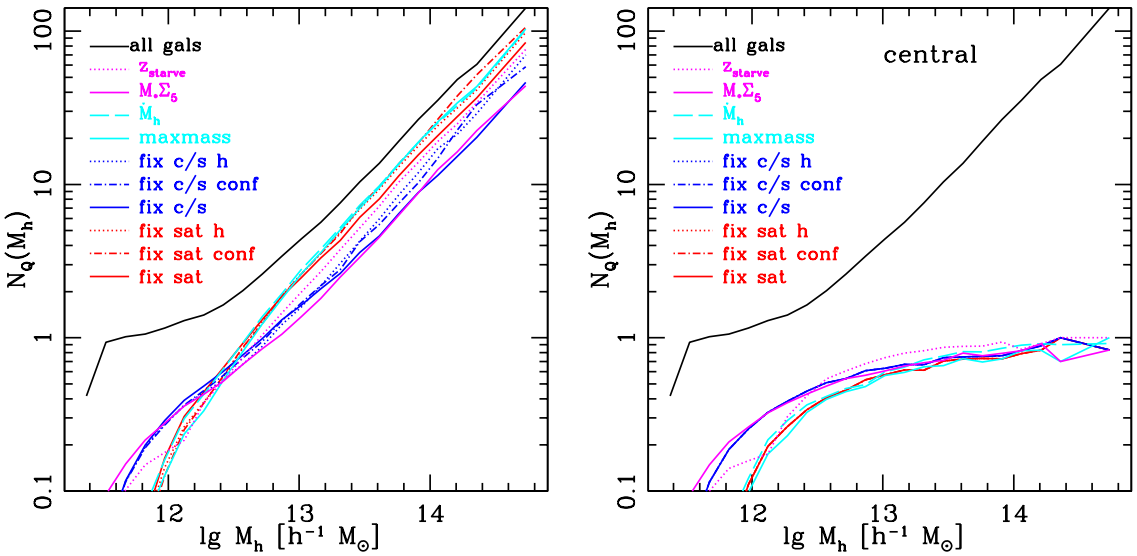

Figure 5. Left: quiescent galaxy HON for our models (line types as in Fig. 2). The top mass bin is wider than the lower ones in order to have at least ten halos in it: the halo to halo scatter can be large, especially in the "-conf" model where changing a central galaxy between quiescent and active in principle changes all the satellites as well. This leads to the features in the dot-dashed, blue "fix c/s-conf" model. Note that the quiescent galaxy richness can vary by a factor of two between models for the highest mass halos, i.e. galaxy clusters. Right: quiescent central galaxy HON. In both panels, the black solid line is the HON of all galaxies.

of host halo mass has implications for the physical role halo environments and membership play in turning galaxies from active to quiescent.

4.3 Quiescent Galaxy Distribution in Clusters

In addition to measuring the number of galaxies in a halo of a given mass, we can ask how these galaxies are distributed within the halos (i.e. the profile). Aside from the $M_\star\,\Sigma_5$ prescription, and to some extent the "-conf" models, spatial properties are not used to define which galaxies are quiescent – so any dependence arises due to correlations with other properties which *are* used in the models.

For the 18 most massive clusters in the simulation ($M_h \geq 2\times10^{14}\,h^{-1}M_\odot$) we stacked the counts of quiescent galaxies in bins of radial distance from the most bound particle within the halo (which is very close to the minimum of the halo potential and the density peak). We used logarithmically spaced bins in $r/r_{\rm vir}$, where $r_{\rm vir}$ is the virial radius[14]. The total number of quiescent galaxies in clusters changes from model to model, as already shown in Fig. 5. To highlight the additional information given by the profile, we normalize the stacked counts for each model at $r = r_{\rm vir}$. The resulting profiles are shown in Fig. 6.

In all of the models the quiescent galaxy radial profiles tend to be more centrally concentrated than those of all galaxies (the solid black line), reminiscent of the well-known morphology- and color-density relations (e.g. Dressler et al 1997; Treu et al 2003; Balogh et al 2004; Kauffmann et al 2004; Postman et al 2005; Christlein & Zabludoff 2005; Loh et al 2008; Skibba et al 2009; Cibinel et al 2013; Lackner & Gunn 2013; Muzzin et al. 2012). Amongst the models, the "fix c/s-h" and $z_{\rm starve}$ models are the most centrally concentrated (this increase in concentration is due to a quicker drop off in quiescent galaxy density at high radius compared to many of the other models). The weak but non-zero correlation between infall time and radius (Oman, Hudson & Behroozi 2013)[15] imprints a radial dependence for the $z_{\rm starve}$ model. The large number of quiescent galaxies in the $M_\star\,\Sigma_5$ model near the cluster centers is a direct consequence of the increase of the quiescent fraction with projected density (Eq. 4).

5 COMPARISONS: OBSERVATIONAL

In summary, the models produce different numbers of quiescent centrals and satellites, place them in different halos (HON) and in different places in halos (profile). These results are very useful for understanding the differences between the models but are challenging to access observationally. They do however drive differences in quantities which can be probed observationally, for example the change in the HON leads to changes in the galaxy correlation function or in the richness distribution of groups. We now turn to such statistics and describe how the differences we have seen above translate into differences in the observables.

[14] We take $r_{\rm vir} = 0.92\,r_{180b}$, where r_{180b} is the radius at which the average density within the cluster reaches 180 times the average background density. This radius is measured from the halo center using all of the particles in the simulation (not just group members). The factor 0.92 is the conversion between r_{180b} and $r_{\rm vir}$ for a $c = 4$ Navarro, Frenk & White (1996) halo at $z = 0.5$, calculated as described in White (2001).

[15] Also, Wetzel et al to appear.

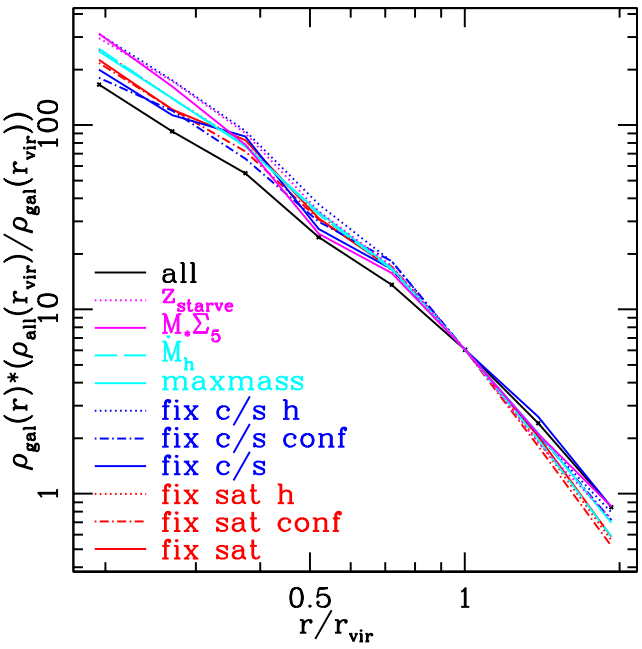

Figure 6. Quiescent galaxy radial profile, for the 18 $z \simeq 0.5$ clusters with $M \geq 2 \times 10^{14}\, h^{-1} M_\odot$, rescaled at $r = r_{\rm vir}$ to agree with the total galaxy distribution (black line). Line types are as in Fig. 2.

5.1 Quiescent galaxy correlation function

One of the most basic measurements that can be made on any population of objects is its two-point correlation function. In recent years it has become standard to use measurements of the correlation function to infer the halo occupation distribution (shown in Fig. 5). We thus expect the correlation function to be a useful diagnostic of these models.

5.1.1 Auto-correlations

We use the Landy & Szalay (1993) estimator to measure the (auto-)correlation functions for our catalogs. The results for the real-space correlation function are shown at the top of Fig. 7, with the ratios of each model to the full galaxy real-space correlation function below (to highlight the differences between models). Errors are shown for only 4 cases to avoid clutter in this and subsequent figures. The box is split into octants to compute the errors, which represent the error in the mean of the octants. They thus indicate how well a survey of comparable volume to our box could determine $\xi(r)$.[16] Clearly, several of our prescriptions cleanly separate with a volume comparable to our simulation. The difference between the curves in comparison to the errors can be used to indicate the observational requirements to distinguish them.

The correlation function trends are as expected from the halo occupations in Fig. 5: models with more galaxies in higher mass halos cluster more strongly on both large and small scales. The large-scale clustering is set by the bias, which is determined by the mean, galaxy-weighted, halo mass. The small-scale clustering is set by the number of central-satellite and satellite-satellite pairs within a single halo. Satellites with the longest time since infall (taken as quiescent for "fix sat-h") or since maximum mass (taken as quiescent for "maxmass") reside in the most massive clusters, so the corresponding quiescent samples cluster more strongly than the randomly chosen quiescent galaxy sample does. In addition, the "-conf" models tend to put more quiescent satellites in high mass halos, as most of the high mass halo central galaxies are quiescent. (This model also has the largest variance as changing one central galaxy to or from quiescent in a rare halo can significantly change the number of quiescent satellites for that halo mass and thus the number of quiescent galaxies with many nearby neighbors. This suggests that surveys aimed at ruling out this model need to sample a large volume with a representative sample of high-mass halos.)

The impact of the radial profile within massive halos on $\xi(r)$ is not very strong. While the models separate in Fig. 6 we see two degeneracies seen in the HON in $\xi(r)$ as well: the $M_\star\, \Sigma_5$ and random"fix c/s" models, and $\dot{M}_h$ and "fix sat-h" models are also close (the latter two have significant overlap in their populations as mentioned earlier).

In practice the three dimensional real-space correlation function is found by "deprojecting" either the projected correlation function (to minimize the influence of redshift-space distortions) or the angular correlation function (if only coarse distance estimates are available). If accurate redshifts are available for the galaxies, the redshift space correlation function can in principle carry additional information, at least in part because the small-scale clustering is affected by fingers-of-god and thus is sensitive to the satellite fraction in massive halos. To bring the comparison closer to the observational plane, the projected correlation function

$$w_p(r_p) = \int_{-z_{\rm cut}}^{z_{\rm cut}} \xi(r_p, z)\, dz \qquad (5)$$

is shown in Fig. 8, where we see it exhibits similar behavior to $\xi(r)$. In Eq. (5), r_p is the separation in the plane of the sky, z is the separation along the line-of-sight in redshift space and $z_{\rm cut}$ is a cutoff in the line-of-sight direction. Ideally $z_{\rm cut}$ is very large so that the the cutoff doesn't matter, however, our $125\, h^{-1}$Mpc on-a-side octants are relatively small which argues against using very large $z_{\rm cut}$. One can still define and measure $w_p(r_p)$ with a small $z_{\rm cut}$, but the $z_{\rm cut}$ should be matched when comparing theory and observation. Throughout we use $z_{\rm cut} = 25\, h^{-1}$Mpc, thus considering cylinders $50\, h^{-1}$Mpc deep in the redshift (velocity plus position) direction within each of the eight $125\, h^{-1}$Mpc octants in the box.

We also computed the angle-averaged, or monopole, redshift correlation function, $\xi(s)$. The trends and differences between the models in $\xi(s)$ closely followed those seen in $\xi(r)$, indicating that both statistics are comparable in their discriminating power and the additional sensitivity to e.g. the fingers-of-god is small. (The most noticeable difference in $\xi(s)$ is that the "fix c/s-conf" model increases its

[16] While we primarily show real space auto-, cross- and marked correlations here and below, the trends we focus on are possible from combinations of their redshift space counterparts such as Fig. 8, as well as being accessible via construction of real space quantities themselves.

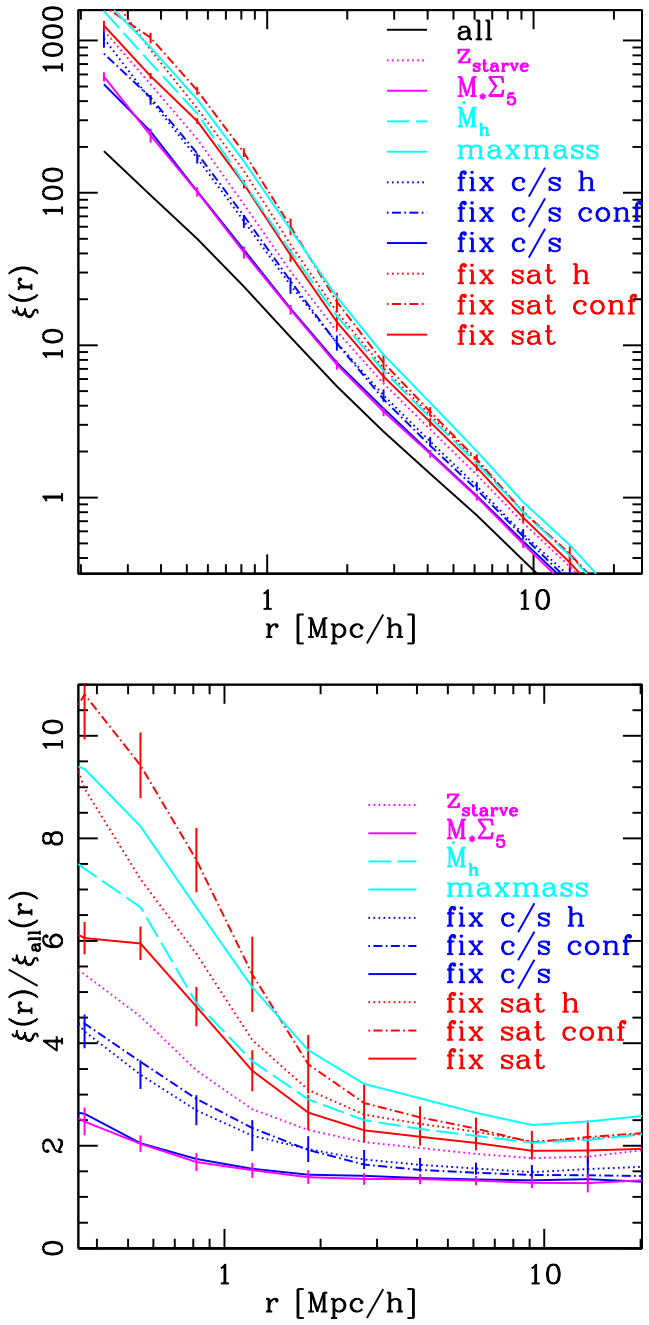

Figure 7. Top: three dimensional real-space correlation function, $\xi(r)$. The solid black line is the correlation function of all galaxies, $\xi_{\rm all}(r)$; other line types are as in Fig. 2. For clarity, representative error bars are shown only for four examples. Just as in the HON, the $M_\star\Sigma_5$ model and random "fix c/s" models are roughly degenerate, as are the $\dot{M}_h$ and "hist sat" models (which have $\sim 80\%$ overlap in their populations). The strongest clustered prescription at short distances (red dot-dashed line) is "fix sat conf", i.e. the galactic conformity model with the larger number of quiescent satellites, as expected again from the HON. The $z_{\rm starve}$ quiescent galaxy correlation lies between the other two sets of trends, again as expected from the HON in Fig. 5. Bottom: $\xi(r)/\xi_{\rm all}(r)$ for each quiescence prescription, which highlights differences between the models. Note the linear vertical scale.

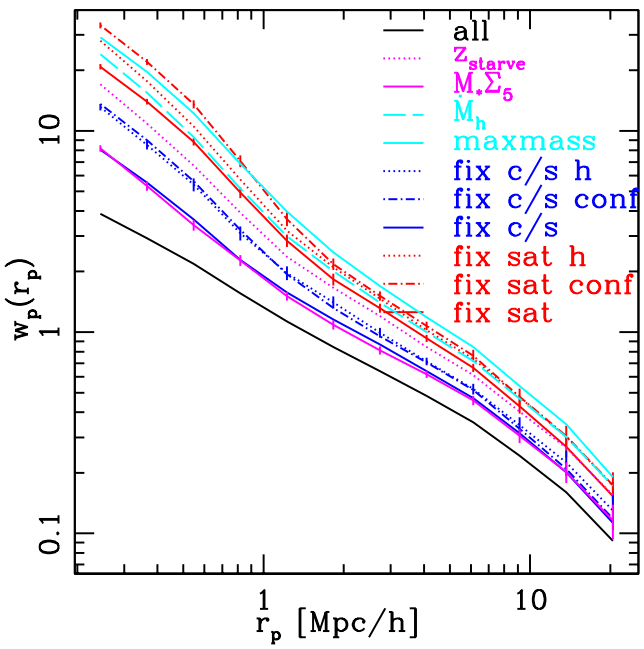

Figure 8. Projected correlation function, w_p, for same 10 models as in Fig. 2, integrating over $\pm 25\,h^{-1}$Mpc in the redshift direction. The model separations are similar to those seen in the isotropic three dimensional correlation function (Fig. 7, top).

relative clustering at low separation, making it easier to differentiate it from the "fix c/s-h" model.)

5.1.2 Cross-correlations

While it is not as commonly employed, it is also possible to measure the cross-correlation[17] between quiescent and star-forming galaxies (or between either population and the full sample). As an example we show the cross-correlation function, $\xi_\times(r)$, between quiescent and star-forming galaxies at top in Fig. 9. The differences between models are not large, and appear mostly at small scales. This cross-correlation is most useful in testing the models which invoke conformity (especially the "fix sat-conf" model from the rest). Models which exhibit galactic conformity have fewer pairs of quiescent and star-forming galaxies within a single halo (preferring to have all of one type, the same as the central) so the cross-correlation is suppressed on small scales. The trend is less pronounced in the "fix c/s-conf" model, which has more halos where central and satellite galaxy quiescence are mismatched. The cross correlation divided by a reference power law model, shown in the lower half of Fig. 9, more clearly separates the models.

We also show the projected cross correlation function in Fig. 10. It is defined analagously to Eq. 5 and again limited to small $z_{\rm cut} = 25\,h^{-1}$Mpc in the redshift direction because of our box size.

[17] We thank F. van den Bosch for suggesting this measurement.

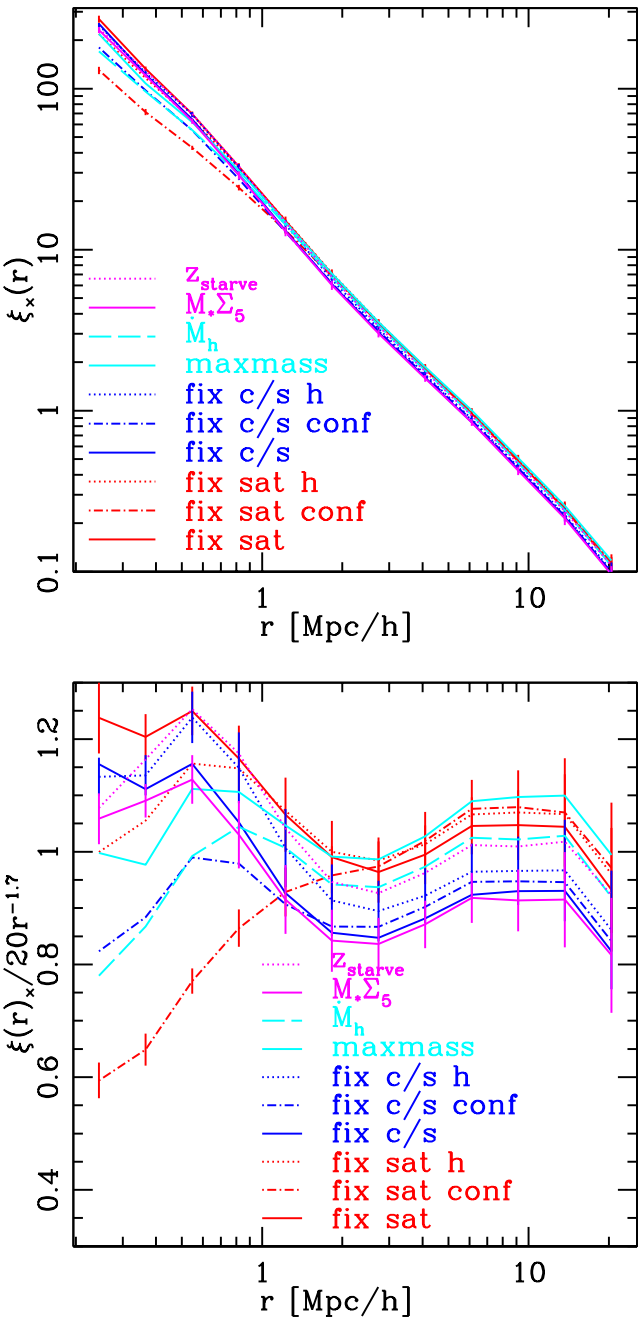

Figure 9. Top: Three dimensional cross-correlation function between quiescent and active galaxies for each catalogue. Line types are as in Fig. 2. The "fix sat-conf" model most clearly separates out from the others at small separations. Bottom: Dividing by a reference power law model, $\xi_{\rm ref}(r) = 20(r[Mpc/h])^{-1.7}$. Just as in the auto-correlation function, this highlights differences between the models, although due to the larger error bars many differences here are not significant.

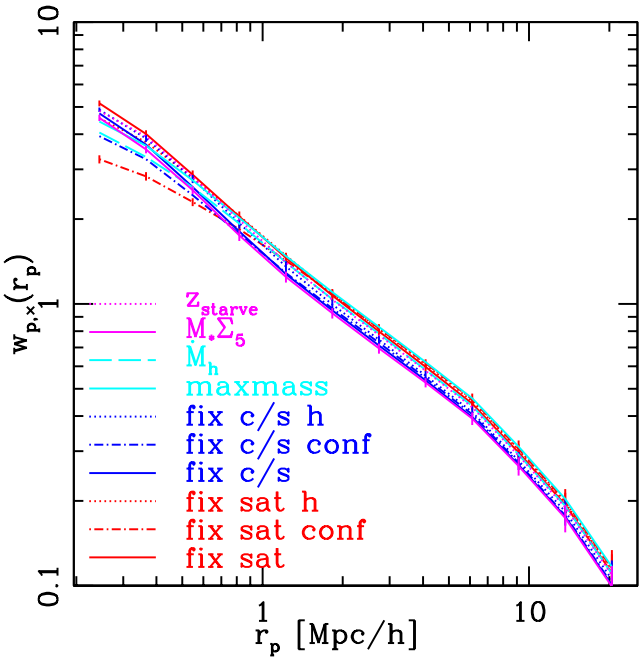

Figure 10. Projected ($\pm 25\,h^{-1}$Mpc in redshift space) cross-correlation function between quiescent and active galaxies for each catalogue, showing similar trends to its isotropic counterpart at top in Fig. 9. Line types are as in Fig. 2.

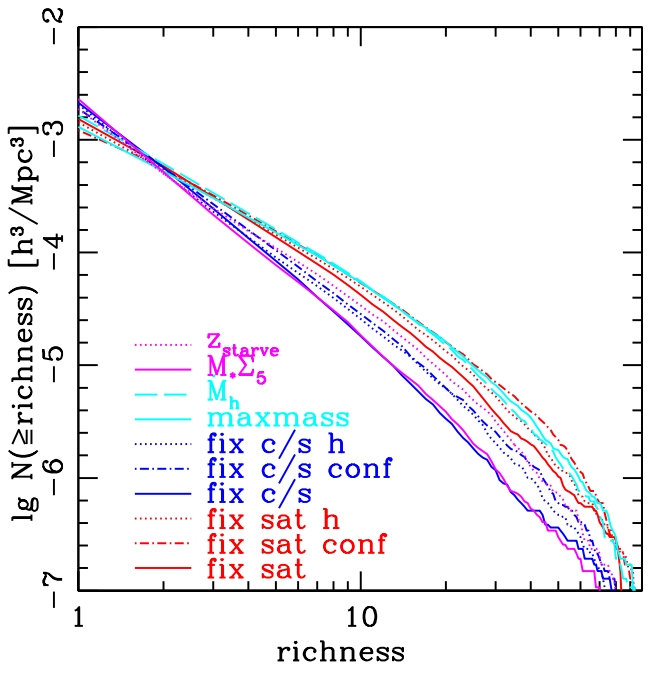

Figure 11. Group multiplicity function (the number density of groups with N or more quiescent galaxies) for the mocks with line types as in Fig. 2. Groups are defined using a redshift space Friends-of-Friends algorithm as discussed in the text.

5.2 Group multiplicity function

One way to constrain the manner in which galaxies occupy halos is to model the galaxy correlation function, assuming a particular profile and parameterized halo occupation distribution. An alternative method is to measure the number of groups of objects of a given richness, i.e. the group multiplicity function. Differences between models or between models and observations are of course easier to interpret the more closely the richness measure (or other observable) tracks halo mass, but even relatively coarse measures can be interpreted with the aid of mock catalogs.

There are numerous methods for constructing group catalogs, which rely on a wide array of differing assumptions. It is not our intention here to perform an exhaustive comparison, but rather to illustrate the potential of this measurement as a diagnostic. For our example we assume we have redshifts for each of our quiescent galaxies and find groups using a Friends-of-Friends algorithm in redshift space (e.g. Huchra & Geller 1982). We follow Berlind et al. (2006, see also Hearin et al. 2013a, who used it to study abundance matching) and set the linking lengths in the line-of-sight and perpendicular directions as $b_\perp = 0.14$ and $b_\parallel = 0.75$, both measured in units of the mean inter-galaxy separation and including only quiescent galaxies in the input catalog. We define richness to be the number of (quiescent) galaxies associated with each group. Fig. 11 shows the cumulative number density of groups as a function of richness, for the different catalogs.

The basic trends in Fig. 11 can be understood by reference to the HON in Fig. 5. The "fix c/s" and $M_\star\,\Sigma_5$ models have the fewest rich groups, because they have the fewest quiescent galaxies per massive halo (Fig. 5). By contrast the "maxmass" and "fix sat-conf" models, which have many quiescent galaxies in massive halos, have a relatively large number density of rich groups. In general we see that the imperfections involved in constructing the group finder (i.e. the impurity and incompleteness) do not qualitatively change the trends present in the underlying models. This suggests that a sufficiently accurate group catalog would provide a strong discriminant between the models. Because it opens up a large parameter space, we leave an examination of other group finding methods, and methods which can work with photometric redshifts, for future work.

5.3 Two dimensional profile in clusters

One can also consider the observational counterpart of the three dimensional cluster profile (Fig. 6), the two dimensional cluster profile. Here galaxies are counted within a redshift cylinder of the cluster center. However, accurately estimating the observational scatter is more challenging with our mock catalogues, as it relies upon the accuracy of the cluster mass (determining $r_{\rm vir}$) and cluster centering, both of which include significant assumptions besides those used in the construction of the catalogue. To bound the information one could obtain from this measurement we consider the case where the group center and $r_{\rm vir}$ are known perfectly. In this limit the most notable distinction this measurement provides is between the $M_\star\,\Sigma_5$ and "fix c/s" models. However as we will see below, this can be obtained with other more direct observations.

5.4 Distribution of projected density: Σ_5

The $M_\star\,\Sigma_5$ model of Peng et al. (2010) used a projected density, Σ_5, in determining which galaxies are classified as quiescent. This is a property that can be used to help discriminate amongst models, even when the models make no explicit reference to it. There are many types of density one could define (for a comparison, see, e.g., Haas, Schaye & Jeeson-Daniel (2012); Muldrew et al. (2012)), we shall consider Σ_5 because it has been studied in this context by Peng et al. (2010) and is used as input to one of our models.

The distribution of Σ_5 across the whole galaxy sample is approximately lognormal, as expected. However the distributions of Σ_5 for the quiescent galaxies, in raw counts and as a fraction of all galaxies (Fig. 12), discriminate quite strongly among the models. Models split into two groups, mostly determined by the quiescent satellite fraction as a function of stellar mass. Models with a large number of quiescent central galaxies tend to have overall more galaxies at lower Σ_5 (Fig. 12, top). (Central galaxies are a minority population for high densities, only reaching at least half of the galaxies for projected densities $\lesssim 10$.) A slightly different division between the models is seen in the quiescent galaxy fraction (Fig. 12, bottom). Differences become the most pronounced at the high density tail ($\Sigma_5 \gtrsim 10^2$), composed almost entirely of satellites in rich groups or clusters. The general shape of the quiescent fraction (Fig. 12, bottom) is expected: the rise of the quiescent fraction to high $M_\star$ implies that higher $M_\star$ satellites are generally quiescent and such satellites lie predominantly in massive halos.

The "fix c/s" model has the lowest quiescent fraction at

high Σ_5 – Eq. (2) requires many low-$M_\star$, central galaxies to be quiescent. This means the satellite galaxies in the same $M_\star$ bin must be star-forming, removing the high-Σ_5 population in Fig. 12. The "fix c/s-conf" model favors galaxies in high mass halos with a star-forming central to be star-forming, removing quiescent galaxies from these high density halos. This is somewhat counteracted for the "fix c/s-h" models as the longest lived satellites tend to be in the higher mass halos. The $M_\star$ Σ_5 model has the highest quiescent fraction for highest Σ_5, partly by construction. Next highest are the "fix sat-h", $\dot{M}_h$ and "maxmass" models. These models turn galaxies quiescent based upon infall time and galaxies that fell in earlier tend to be in higher mass halos and thus denser environments.

In is encouraging that two models which were quite close in their HON, $M_\star$ Σ_5 and "fix c/s", separate cleanly by looking at the high projected density tail of the quenched fraction.

5.5 Marked Correlation Functions

In addition to looking at the distribution of Σ_5, we can use the projected density as a weight when computing the two point function, creating a "marked" correlation function (Sheth, Connolly & Skibba 2005; Harker et al. 2006; Skibba et al 2013). Such a function is straightforward to compute if $\xi(r)$ can be computed and can be used to break degeneracies in modeling the occupation distribution (White & Padmanabhan 2009).

The marked correlation function, $M(r)$, is defined as

$$M(r) = \frac{1}{n(r)\bar{m}^2} \sum_{ij} m_i m_j \qquad (6)$$

where the sum is over all galaxy pairs, i and j, which are separated by r and m_i and m_j are the marks, $n(r)$ is the number of pairs in the bin and $\bar{m}$ is the average mark in the sample. $M(r) \neq 1$ on scales where the clustering of objects depends upon the mark. One of the advantages of a marked correlation function, from an observational perspective, is that it is simple to modify a code which computes $\xi(r)$ to also compute $M(r)$. No further information is needed (beyond the marks and galaxy positions). In fact, one does not even need a random catalogue due to the cancellation between the numerator and denominator. It is also relatively easy to estimate the errors (Sheth, Connolly & Skibba 2005). We will focus here on the three dimensional marked correlation function but there is no reason one cannot use the projected or angular version instead.

If we take our mark, m_i, to be the projected density Σ_5 of the ith galaxy, the resulting $M(r)$ is shown in Fig. 13. For comparison, we also show the marked correlation function for all (not just quiescent) galaxies as the solid black line. As expected, the $M_\star$ Σ_5 quiescent galaxies cluster differently, as the mark Σ_5 was used in their selection. There is a feature between 1 and $2\,h^{-1}$Mpc, roughly at the virial radius of massive halos. Some similarities between the model ordering at small radius and the stacked and rescaled cluster profiles (Fig. 6) is apparent.

If the dynamic range in the mark is very large, then there is some concern that $M(r)$ can become sensitive to rare outliers. A simple way around this is to modify the mark from Σ_5 to

$$\widetilde{\Sigma} \equiv \frac{\Sigma_{\rm max}\ \Sigma_5}{\Sigma_{\rm max} + \Sigma_5} \qquad (7)$$

with $\widetilde{\Sigma} \simeq \Sigma_5$ for $\Sigma_5 \ll \Sigma_{\rm max}$ and $\widetilde{\Sigma} \leq \Sigma_{\rm max}$. Fig. 12 suggests that $\Sigma_{\rm max} = 300$ is a reasonable choice, and we take that as our fiducial value. The resulting $\widetilde{M}(r)$ is shown in Fig. 14. Similar behavior is seen as we vary $\Sigma_{\rm max}$ from 30 to 300 suggesting the features we see in Fig. 13 are stable and robustly present in the catalogs. As $M(r)$ and $\widetilde{M}(r)$ combine projected density and galaxy number, an enhancement at small scales could be due to many galaxies with a small mark, or few galaxies with a large mark. To differentiate, we removed the 3-7 per cent of galaxies with $\Sigma_5 \geq 10^2$ from the catalog. This only decreases the radius below which these models dominate (to $\sim 800\,h^{-1}$kpc/h), but does not erase the separation. Thus we infer the small-scale enhancement

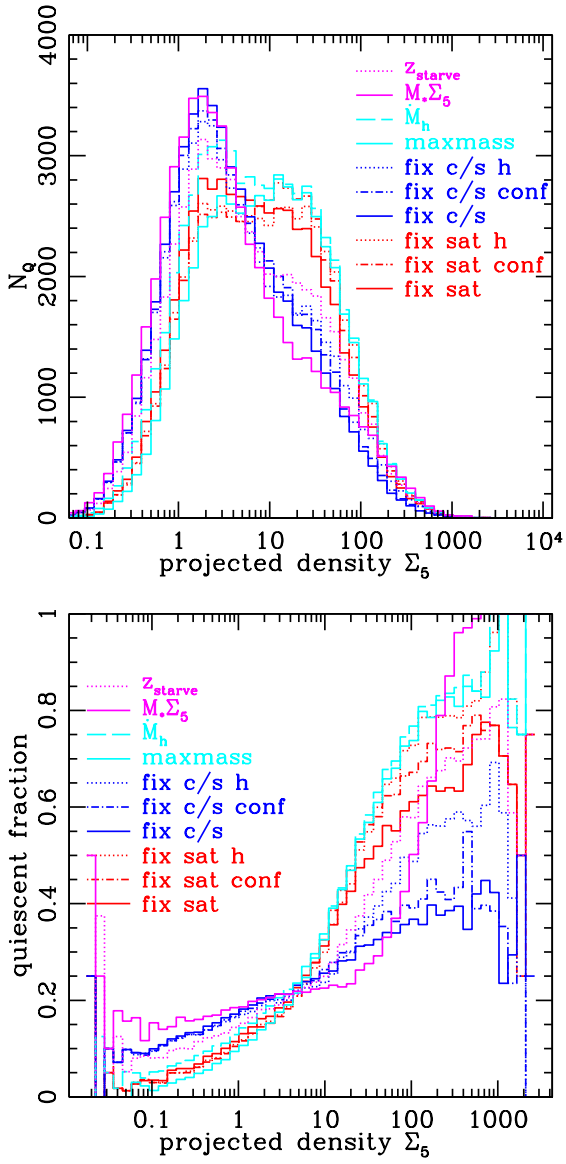

Figure 12. Total number (top) and fraction (bottom) of quiescent galaxies at a given projected density, Σ_5, which are quiescent. Line types as in Fig. 2.

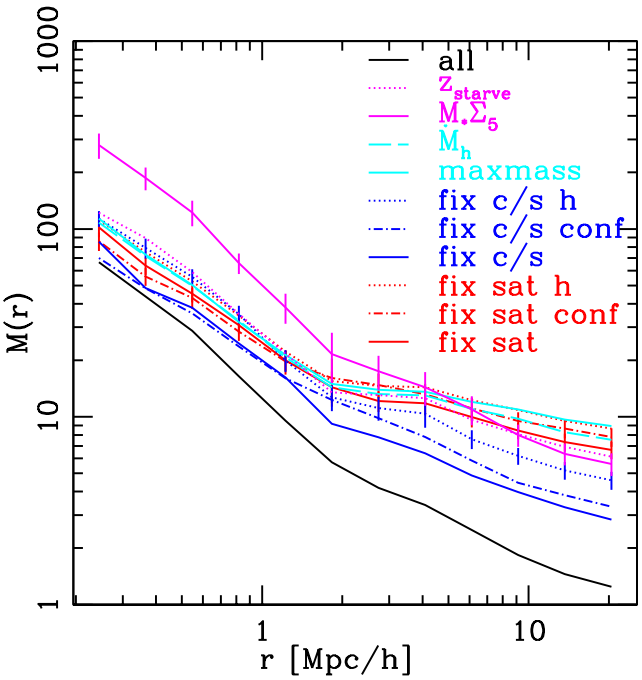

Figure 13. Marked correlation function, $M(r)$, for quiescent galaxies. Line types are as in Fig. 2 and the solid black line is $M(r)$ for all galaxies. The mark is the $5^{\rm th}$ nearest neighbor projected density, Σ_5, of Peng et al. (2010). Error bars indicate the error on the mean $M(r)$ from 8 disjoint octants of the box. The $M_\star\,\Sigma_5$ models separates out cleanly from the others.

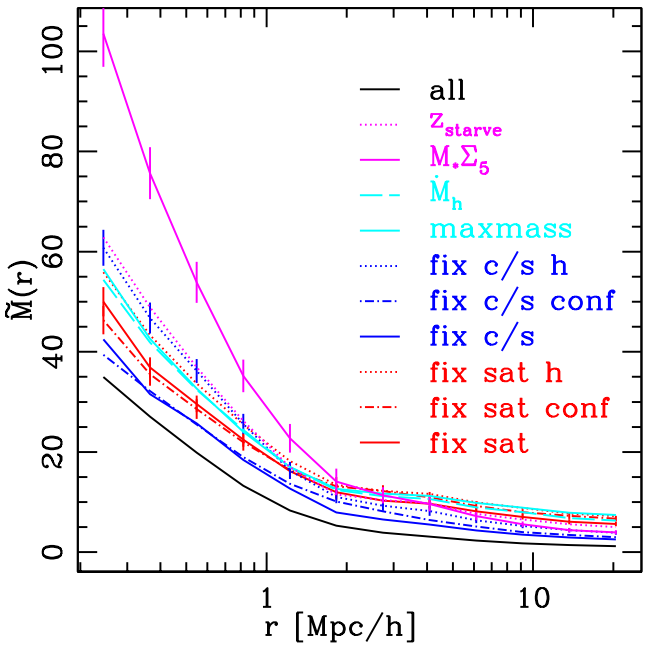

Figure 14. Marked correlation function, $\widetilde{M}(r)$, for quiescent galaxies using Eq. (7) as the mark with $\Sigma_{\rm max} = 300$. Line types are as in Fig. 13 and the solid black line is $\widetilde{M}(r)$ for all galaxies.

is driven by a large number of galaxies, not simply the dense tail of the distribution.

In this section we considered several observational measurements and how they separated out the different quiescent galaxy catalogues. Now we turn to general results and implications of the intrinsic and observational measurements the the ensemble of catalogues.

6 DISCUSSION

We generated a set of mock galaxies by assigning stellar masses to subhalos in an N-body simulation via abundance matching. These mock galaxies match, by construction, the stellar mass function of Drory et al. (2009), as shown in Fig. 1. We then marked a fraction of these galaxies as quiescent, using 10 prescriptions adapted from the literature. All of the prescriptions are tuned give a good fit to the total quiescent fraction as a function of $M_\star$, as shown in Fig. 2, but differ in their assumptions about which properties are important in determining quiescence and in how they incorporate centrality, environment and history.

The number of implied quenching mechanisms differs as well. Two are used in the "fix sat", "fix sat-h","fix c/s", "fix c/s-h" models (for satellite and for central galaxies), and for the $M_\star\,\Sigma_5$ model (stellar mass and projected density), while "fix sat-conf", "fix c/s-conf" might allow one mechanism across a shared halo. The "maxmass", $\dot{M}_h$ models have one mechanism, combined with no mass gains for satellites, while the $z_{\rm starve}$ model has three mechanisms.

We investigated the consequences of these different quiescence assumptions for intrinsic galaxy properties and observational measurements, at one fixed redshift. Models differed in intrinsic properties such as halo occupation and galaxy profiles within massive halos, although the central/satellite split as a function of stellar mass was degenerate for several of them. Observationally, we considered measurements derived from galaxy positions and stellar masses. Promisingly, we found that almost all of the models could be separated from each other by some combination of observations, if measurement errors could be made small enough. While many of the models could be distinguished based on very traditional measurements such as the auto- and cross-correlation functions, we also saw that less often considered statistics such as the group multiplicity function and the (projected) density-marked correlation function allowed us to further break degeneracies between models. We advocate that these statistics be reported in future.

We now turn to intrinsic and observational properties and how they relate to each other and to mechanisms/models for quenching star formation. We saw that the fraction of $\lg M_\star/M_\odot \simeq 10$ quenched galaxies which were central or satellite roughly divided the models into two groups. The strongest division was between different choices for the evolution of the quenched satellite fraction with redshift, as expected, but this division also strongly separated the $M_\star\,\Sigma_5$ model from the ones in which SFR $\propto \dot{M}_h$ or where quiescence was based upon the time at which the subhalo achieved its maximum mass, for example. This division further implied a change in the way quiescent galaxies occupied halos, i.e. the HON (Fig. 5) which showed up clearly in the relative clustering (Fig. 7). This argues that measures of quiescent galaxy clustering can be used to constrain the redshift evolution of the quiescent fraction of satellite and central

galaxies and thus the timescale over which star-formation quenching acts (see also Wetzel et al. 2013a; Tinker et al. 2013, for similar conclusions).

Models which are degenerate in their satellite or central quenched galaxy fractions as a function of stellar mass can still differ significantly in other measures, depending upon environment and history. Those which invoke conformity tend to have the largest number of quiescent satellites in massive halos within their class. Observationally this leads to enhanced auto-correlation, since massive halos have a large bias. These models also have a depressed cross-correlation between active and quiescent galaxies at small separations, as galaxies in a halo tend to all be either active or quiescent. Conformity might point to quenching properties acting on larger scales than those of a halo, as for fixed stellar mass it can give similar quenching likelihoods to satellites at the outskirts and satellites near the center.

The models based upon conformity have central galaxy assignments identical to those of their associated models based on satellite infall or random selection. It was therefore encouraging that there were significant, observable differences associated with the variations in satellite quiescence mechanisms. (This is in part why conformity was introduced at lower redshifts in the SDSS (Ross & Brunner 2009), but here it also separated out the models where satellite infall was related to quiescence.)

The associated "-h" models are best further considered along with the other three models using infall time (where satellite infall stops mass gain or generally increases quiescence probability – our "maxmass", $\dot{M}_h$ and $z_{\rm starve}$ models). If halo growth is considered a proxy for baryonic accretion (and satellite infall a proxy for strangulation, or cessation of baryonic accretion), these can be thought of as "feeding limited" models. Observationally, these five models most prominently group together in the projected density marked correlation functions $M(r)$ and $\widetilde{M}(r)$. They are large at short distances, only being surpassed by the $M_\star\,\Sigma_5$ model (which uses Σ_5 in its construction). This observation thus seems to separate out models which are feeding limited or in which group pre-processing played an important role.

The differences between the three "feeding limited" models which have similar satellite populations ("fix sat-h", "maxmass", $\dot{M}_h$) are interesting as well. All quench satellites after infall (with similar although not identical decay times). The first assigns the central galaxies randomly, while the other two depend upon halo mass gain or time of maximum mass. Differences between these models might thus indicate which intrinsic properties and observations are impacted by the history of central mass gains. (Although the central and satellite quiescent fractions are not identical, in raw numbers there are more differences in the quiescent central populations.) They are quite close in the full HON at high mass, but differ very slightly at low stellar mass (also seen in the central galaxy HON). The three models separate out most clearly (but not by much) from each other in the auto-correlation function. The "maxmass" is slightly larger at high richness in the group multiplicity function, and the $\dot{M}_h$ model also has a relatively depressed quiescent-active galaxy cross-correlation at short distances. Otherwise, the history of central mass gains seems to not have much of an effect on the observations we considered.

All of the models make an explicit distinction between central and satellite galaxies except for the $M_\star\,\Sigma_5$ model. Due to the way it is constructed, this model shows a very different distribution of Σ_5 for quiescent galaxies than the other models, which results in a strong enhancement of the projected density-marked correlation function at small scales, and the quiescent fraction as a function of projected density. In the other observations it is close to degenerate with the model sharing its HON and profile, which assigns quiescent galaxies depending only upon centrality ("fix c/s").

Several observations were quite good proxies for the intrinsic differences we saw between the models. For example, the group multiplicity function we used orders models in almost the same way as the HON at high richness or halo mass (only two models reverse). The two dimensional stacked cluster profile has information similar to the three dimensional stacked cluster profile and the projected density distribution (for $\Sigma_5 \sim 10 - 100$) showed a similar ranking of models to the quiescent satellite fraction at intermediate $M_\star$. If one can reliably infer which galaxies belong to which dark matter halo from a group catalog, and has a reliable method of determining the central galaxy, then the central and satellite quiescent fractions become directly observable. As we saw, these functions were extremely helpful in partitioning the models. Conversely the differences in quiescent fraction at high projected density and differences in the radial profile may impact the calculations of purity and completeness for color-selected cluster finders which are trained on mock catalogs (which make either implicit or explicit assumptions about these properties).

We used ten catalogues with quiescence based upon dark matter subhalo histories, environment and centrality. However, these tests could be expected to shed light on many other proposed models, including those based upon fewer simulation properties (e.g. without subhalos, such as Peacock & Smith 2000; Seljak 2000; Cooray & Sheth 2002), more simulation properties (e.g. including histories, for instance, Wetzel et al. 2013a; Moster, Naab & White 2013; Mutch, Croton & Poole 2013; Cattaneo et al. 2013; Baugh 2006; Benson 2012, or baryons, e.g., Schaye et al. 2010; Almgren et al 2013; Vogelsberger et al. 2013), or other simulation properties (e.g., density as in Scoville et al. 2013). Other tests may also add more information (e.g. lensing was used by Masaki, Lin & Yoshida (2013) for similar tests at lower redshifts, we did not consider it here as galaxy shapes are required as well). Some tests to constrain quiescence were recently reported by Tinker et al. (2013) at similar redshifts (clustering, weak lensing, group catalogue) as this work was being prepared for publication.

7 CONCLUSIONS

One of the most striking features of the galaxy population is that it exhibits bimodality in color, morphology and star-formation rate. In particular, the existence of two broad types of galaxies (those which are actively star-forming and those which are quiescent) cries out for a theoretical explanation. Unfortunately the range of physics and of physical scales involved in setting the star-formation rate in a galaxy is enormous, making empirical models of the phenomenon of great importance. Many such models have been proposed to explain the color or star-formation rate bimodality at

$z \simeq 0$. Motivated by the wealth of data on the higher z Universe which we expect to have soon from large surveys, and using high-resolution cosmological N-body simulations, we have investigated the predictions for a range of models for star-formation quenching to see in what way they differ and what observations (of what accuracy) can be used to discriminate amongst them. The advantage of using large surveys is that statistical errors can be controlled and are more accessible and one can disentangle the many correlations between galaxy properties which limit inferences from small samples. The disadvantage is that information is more circumstantial and so requires a different sort of detective work.

We have focused our attention at $z \simeq 0.5$, which is at high enough z that we expect significant galaxy evolution but low enough z that we expect to have large statistical samples of galaxies in the near future. Note that $z \simeq 0.5$ is approximately 5 Gyr ago, which is longer than the main-sequence lifetime of $> 1.4\,M_{\odot}$ stars. Any galaxy less massive than $2{\times}10^{10}\,M_{\odot}$ on the star forming main sequence would at least double its stellar mass in this period. It is also around $z \simeq 0.5$ that we see a rapid rise in the number density of intermediate-mass, quiescent galaxies, making this a particularly interesting time to study.

We considered several different galaxy properties which are expected to correlate with star-formation quenching and investigated how statistical measurements might be used to distinguish them. We created different mock catalogues, all sharing the same stellar mass for each galaxy and close to the same overall quenched fraction as a function of stellar mass, but with different criteria for classifying a galaxy as quiescent. Many of these models had degeneracies in basic intrinsic properties (satellite/central fraction, for instance), or halo occupation (HON), but the suite of observations we used could nonetheless separate them out, given small enough measurement errors. Fixing the quenched central galaxies and varying the satellite quenching gave models which were distinguishable, similarly, models where the majority of differences were in the central galaxies also could be differentiated.

More specifically, in addition to the quiescent galaxy auto and cross-correlation functions and quiescent fraction as a function of stellar mass, we found that projected density counts, the projected density marked correlation function, and the group multiplicity function could further serve to separate models, and also seemed to correlate with centrality in host halo, feeding limited quenching and halo occupation respectively. These observational measurements increase the galaxy formation information available from surveys possessing galaxy stellar masses and positions.

We have mostly considered how these observational measurements can be used to distinguish models from each other, using observations. Alternatively this provides a particularly discriminating set of tests for validating mock catalogues, constructed by any means. They can also be used to decode associations of other galaxy properties with galaxy histories, environments and centrality, for instance AGN activity or morphology.

While we were completing this work we became aware of Tinker et al. (2013) which compared several different measurements of a survey at similar redshifts to constrain quiescent fraction evolution and of Hearin et al. (2013b) which considered measurements at low redshift to constrain color and developed a formalism for comparing dark matter simulation properties which are correlated with color.

We thank E. Bell, F. van den Bosch, K. Bundy, N. Dalal, C. Knobel, M. George, A. Hearin, C. Heymans, C. Lackner, Z. Lu, P. Behroozi, D. Watson, A. Wetzel for conversations, and D. Watson, A. Hearin, R. Skibba, A. Wetzel and the referee for helpful suggestions on the draft. JDC also thanks the Royal Observatory, Edinburgh, and Kavli IPMU for their hospitality and invitations to speak on this work as it was being completed. JDC was supported in part by DOE. MW was supported in part by NASA.

REFERENCES

Almgren, A., Bell, J., Lijewski, M., Lukic, Z., Van Andel, E., 2013, ApJ, 765, 39
Angulo, R.E., Lacey, C.G., Baugh,C.M., Frenk, C.S., 2009, MNRAS, 3999, 983
Balogh, M.L., Baldry, I.K., Nichol, R., Miller, C., Bower, R., Glazebrook, K., 2004, ApJL, 615, 101
Baugh, C.M., 2006, RPPh, 69, 3101
Behroozi, P.S., Conroy, C., Wechsler, R.H., 2010, ApJ, 717, 379
Behroozi, Wechsler, Conroy, 2013, ApJ, 770, 57
Behroozi, Wechsler, Conroy, 2013, ApJL, 762,31
Benson, A., 2012, New Astronomy, 17, 175
Berlind, A. A., et al., 2006, ApJS, 167, 1
Bruzual, G., & Charlot, S. 2003, MNRAS, 344, 1000
Cattaneo, A., Woo, J., Dekel, A., Faber, S.M., 2013, MNRAS, 430, 686
Christlein, D., Zabludoff, A.I., 2005, ApJ, 621, 201
Cibinel, A., et al., 2013, ApJ, 777, 116
Conroy, C., Wechsler, R., Kravtsov, A.R., 2006, ApJ, 647, 201
Conroy, C., Gunn, J. E., & White, M. 2009, ApJ, 699, 486
Conroy, C., & Gunn, J. E. 2010, ApJ, 712, 833
Conroy, C., White, M., & Gunn, J. E. 2010, ApJ, 708, 58
Cooray, A., Sheth, R., 2002, PhR, 372, 1
van Daalen, M.P., Schaye, J., McCarthy, I.G., Booth, C.M., Dalla Vecchia, C., 2013, preprint [arXiv:1310.7571]
Davidzon et al., 2013, A& A, 558, A23
Davis M., Efstathiou G., Frenk C.S., White S.D.M., 1985, ApJ, 292, 371
Diemand J., Kuhlen M., Madau P., 2006, ApJ, 649, 1
Dressler, A., et al., 1997, ApJ, 490, 577
Drory, N., et al., 2009, ApJ, 707, 1595
Faber S.M., Willmer C.N.A., Wolf C., et al., 2007, ApJ, 665, 265
Fioc, M., Rocca-Volmerange, B., 1997, A&A, 326, 950
Fioc, M., Rocca-Volmerange, B., 1999, astro-ph/9912179
Gerke, B.F., et al., 2012, Ap J, 751, 50
George, M., Ma, C.-P., Bundy, K., Leauthaud, A., Tinker, J., Wechsler, R.H., Finoguenov, A., 2013, ApJ, 770, 113
Guo, Q, White, S.D.M., 2013, preprint [arXiv:1303.3586]
Haas, M.R., Schaye, Joop, Jeeson-Daniel, A., 2012, MNRAS, 419,2133
Harker, G., Cole, S., Helly, J., Frenk, C., Jenkins, A., 2006, MNRAS, 367, 1039,

Hearin, A.P., Zentner, A.R., Berlind, A.A., Newman, J.A., 2013, MNRAS, 433, 659
Hearin, A.P., Watson, D.F., 2013, MNRAS, 435, 1313
Hearin, A.P., Watson, D.F., Becker, M.R., Reyes, R., Berlind, A.A., Zentner, A.R., 2013, arXiv:1310.6747
Heitmann K., et al., 2008, CS&D, 1, 15003
Huchra J.P., Geller M.J., 1982, ApJ, 257, 423
Ilbert O., et al., 2010, ApJ, 709, 644
Kauffmann, G., White, S.D.M., Heckman, T.M., Menard, B., Brinchmann, J., Charlot, S., Tremonti, C., Brinkmann, J., 2004, MNRAS, 353, 713
Kauffmann, G., Li, C., Zhang, W., Weinmann, S., 2013, MNRAS, 430, 1447
Knobel, C., et al., 2013, ApJ, 769, 24
Kovac, K., et al, 2010, ApJ, 708, 505,
Kovac, K., et al, 2013, preprint [arXiv:1307.4402]
Kuhlen, M., Vogelsberge, M., Angulo, R., 2012, Physics of the Dark Universe, 1, 50
Lackner, C.N., Gunn, J.E., 2013, MNRAS, 428, 2141
Landy,S.D., Szalay, A.S., ApJL, 412, 64
Le Borgne, D., et al. 2004, A&A, 425, 881
Lilly S.J., Carollo C.M., Pipino A., Renzini A., Peng Y., 2013, ApJ, 772,119
Loh, Y.-S., Ellingson, E., Yee, H.K.C., Gilbank, D.G., Gladders, M.D., Barrientos, L.F., 2008, ApJ, 680, 214
Lu, Y., Mo, H.J., Weinberg, M.D., Katz, N., 2011 MNRAS, 416, 1949
Lu, Z., Mo, H.J., Lu, Y, Katz, N., Weinberg, M., van den Bosch, F.C., Yang, X., 2013, preprint [arXiv:1306.0650]
Maraston, C., 2005, MNRAS, 362, 799
Marchesini, D., van Dokkum, P.G., Forster Schreiber, N.M., Franx, M., Labbe, I., Wuyts, S., 2009, ApJ, 701, 1765,
Marulli, F., et al., 2013, A & A, 557, 17
Masaki, S., Lin, Y-T, Yoshida, N., 2013, preprint [arXiv:1301.1217],
Mo, H., van den Bosch, F., White, S.D.M., 2010, *Galaxy Formation and Evolution*, Cambridge University Press
Moster, B.P., Somerville, R.S., Maulbetsch, C., van den Bosch, F.C., Maccio, A.V., Naoob, T., Oser, L., 2010, ApJ, 710, 903
Moster, B.P., Naab, T., White, S.D.M., 2013, MNRAS, 428, 3121
Moustakas, J., et al., 2013, ApJ, 767, 50
Muldrew, S.I., et al, 2012, MNRAS, 419, 2670
Mutch, S.J., Croton, D.J., Poole, G.B., 2013, MNRAS, 435, 2445
Muzzin, A., Marchesini, D., van Dokkum, P.G., Labbe, I., Kriek, M., Franx, M., 2009, ApJ, 701, 1839
Muzzin, A., et al, 2012, ApJ, 746, 188
Navarro J., Frenk C.S., White S.D.M., 1996, ApJ, 462, 563
Neistein, E., Weinmann, S.M., 2010, MNRAS, 405, 2717
Oman, K.A., Hudson, M.J., Behroozi, P.S., 2013, MNRAS, 431, 2307
Onions, J., et al, 2012, MNRAS, 423, 1200
Peacock, J.A., Smith, R.E., 2000, MNRAS, 318, 1144
Peng, Y.-J., et al., 2010, ApJ, 721, 193
Perez-Gonzalez, P.G., et al, 2008, ApJ, 675, 234
Phillips, J.I., Wheeler, C., Boylan-Kolchin, M., Bullock, J.S., Cooper, M.C., Tollerud, E.J., 2103, preprint [arXiv:1307.3552]
Postman, M., et al., 2005, ApJ, 623, 721
Pozzetti, L, et al, 2010, A&A 523, A 13
Reddick, R.M., Wechsler, R.H., Tinker, J.L., Behroozi, P.S., 2013, ApJ, 771, 30
Ross, A.J., Brunner, R.J., 2009, MNRAS, 399, 878
Schaye, J., et al., 2010, MNRAS, 402, 1536
Scoville, N., et al., 2013, APJS, 206, 3
Seljak, U., 2000, MNRAS, 318, 203
Sheth, R.K., Connolly, A.J., Skibba, R., 2005, astro.ph/0511773
Simha, V., Weinberg, D.H., Dave, R., Gnedin, O.Y., Katz, N., Keres, D., 2009, MNRAS, 399, 650
Simha, V., Weinberg, D. H., Dave, R., Fardal, M., Katz, N., Oppenheimer, B. D., 2012, MNRAS, 423, 3458
Skibba R.A., Sheth R.K., 2009, MNRAS, 392, 1080
Skibba, R.A., et al., 2009, MNRAS, 399, 966
Skibba, R. A., Sheth, R. K., Croton, D. J., Muldrew, S. I., Abbas, U., Pearce, F. R., Shattow, G. M., 2013, MNRAS, 429, 458
Springel V., Yoshida N., White S. D. M., 2001, New Astronomy, 6, 51
Tinker, J.L., Wetzel, A.R., 2010, ApJ, 719, 88
Tinker, J.L., et al., 2012, ApJ, 745,16
Tinker, J.L., Leauthaud, A., Bundy, K., George, M.R., Behroozi, P., Massey, R., Rhodes, J., Wechsler, R., 2013, preprint [arXiv:1308.2974]
Treu, T., Ellis, R.S., Kneib, J.-P., Dressler, A., Smail, I., Czoske, O., Oemler, A., Natarajan, P., 2003, ApJ, 591, 53
Vale, A., Ostriker, J.P., 2006, MNRAS, 371, 1173
Vogelsberger, M., Genel, S.,Sijacki, D., Torrey, P., Springel, V., Hernquist, L., 2013, preprint [arXiv:1305.2913]
Watson, D.F., Conroy, C., 2013, AjP, 772, 139
Wechsler, R.H., Bullock, J.S., Primack, J.R., Kravtsov, A.V., Dekel, A., 2002, ApJ, 568, 52
Weinberg, D.H., Colombi, S., Dave, R., Katz, N., 2008, ApJ, 678, 6
Weinmann, S.M., van den Bosch, F.C., Yang, X., Mo, H.J., 2006, MNRAS, 366, 2
Wetzel, A.R., Cohn, J.D., White, 2009, MNRAS, 395, 1376
Wetzel, A.R., White, M., 2010, MNRAS, 403, 1072
Wetzel, A. R., Tinker, J.L, Conroy, C., van den Bosch, F.C., 2013a, MNRAS, 432, 336
Wetzel, A. R., Tinker, J.L, Conroy, C., van den Bosch, F.C., 2013b, preprint [arXiv:1303.7231]
White M., 2001, A&A, 367, 27
White M., 2002, ApJS, 143, 241
White, M., Padmanabhan, N., 2009, MNRAS, 395, 2381
White, M., Cohn, J.D., Smit, R., 2010, MNRAS, 408, 1818
Yang, X., Mo, H.J., van den Bosch, F.C., Zhang, Y., Han, J., 2012, ApJ, 752, 41
York D.G., et al., 2000, AJ, 120, 1579
Zentner, A.R., Hearin, A.P., van den Bosch, F.C., 2013, arXiv:1311.1818